Synthetic Analogues of the Active Sites of Iron–Sulfur Proteins. 14.[1] Synthesis, Properties, and Structures of Bis(*o*-xylyl-α,α'-dithiolato)ferrate(II,III) Anions, Analogues of Oxidized and Reduced Rubredoxin Sites

R. W. Lane,[2a] James A. Ibers,*[2b] R. B. Frankel,*[2c] G. C. Papaefthymiou,[2c] and R. H. Holm*[2a]

Contribution from the Departments of Chemistry, Stanford University, Stanford, California 94305, and Northwestern University, Evanston, Illinois 60201, and the Department of Chemistry and Francis Bitter National Magnet Laboratory, Massachusetts Institute of Technology, Cambridge, Massachusetts 02139.
Received June 3, 1976

Abstract: To complete the set of synthetic analogues corresponding to the three known types of active sites in iron–sulfur redox proteins, bis(*o*-xylyl-α,α'-dithiolato)ferrate(II,III) anions, $[Fe(S_2\text{-}o\text{-}xyl)_2]^{2-,-}$, have been prepared and their structures and certain electronic properties determined. These complexes are shown to be related to the active sites of the 1-Fe rubredoxin (Rd) proteins. $(Et_4N)[Fe(S_2\text{-}o\text{-}xyl)_2]$ crystallizes in the orthorhombic space group $C_{2v}{}^9\text{-}Pn2_1a$ of dimensions a = 13.413 (8), b = 29.554 (17), and c = 13.448 (10) Å with Z = 8. $Na(Ph_4As)[Fe(S_2\text{-}o\text{-}xyl)_2]$ acetonitrile solvate crystallizes in the triclinic space group $C_i{}^1\text{-}P\bar{1}$ of dimensions a = 13.67 (1), b = 14.60 (1), c = 11.59 (1) Å, α = 109.3 (1), β = 105.6 (1), and γ = 71.6 (1)° with Z = 2. Both complexes contain high-spin mononuclear anions whose $Fe\text{-}S_4$ coordination units are degraded from T_d symmetry by rhombic distortions. Solution absorption spectra of $[Fe(S_2\text{-}o\text{-}xyl)_2]^-$ (λ_{max} 354, 486, ~640–690 nm) and $[Fe(S_2\text{-}o\text{-}xyl)_2]^{2-}$ (λ_{max} 322, ~355, 1800 nm) resemble those of Rd_{ox} and Rd_{red}, respectively. The same comment applies to Mössbauer parameters (isomer shift, quadrupole splitting) at 77 K: $[Fe(S_2\text{-}o\text{-}xyl)_2]^-$, 0.13, 0.57 mm/s; $[Fe(S_2\text{-}o\text{-}xyl)_2]^{2-}$, 0.61, 3.28 mm/s. Internal hyperfine magnetic field data are also presented for these two complexes. As for Rd_{red} the ground state of $[Fe(S_2\text{-}o\text{-}xyl)_2]^{2-}$ has d_{z^2} symmetry and is separated from the next orbital state by ~900 cm^{-1}. Comparison of structural and collective electronic properties with those of the proteins indicates an extent of correspondence sufficient to designate $[Fe(S_2\text{-}o\text{-}xyl)_2]^-$ and $[Fe(S_2\text{-}o\text{-}xyl)_2]^{2-}$ as analogues of the active sites of Rd_{ox} and Rd_{red}, respectively. Analogue structures are considered to represent close approaches to unconstrained protein site stereochemistries; further comparison between $[Fe(S_2\text{-}o\text{-}xyl)_2]^-$ and Rd_{ox} awaits final refinement of the protein structure. Also prepared in this work are salts of $[M_2(S_2\text{-}o\text{-}xyl)_3]^{2-}$, M = Fe(II) and Ni(II), and $[Co(S_2\text{-}o\text{-}xyl)_2]^{2-}$. The spectrum of the latter together with published data is used to demonstrate the weak ligand field nature of $S_2\text{-}o\text{-}xyl^{2-}$, which is comparable to that of N_3^-, OH^-, and $-NCO^-$. Comparison of the two analogue structures allows an estimate of structural change at the Rd site in the absence of protein constraints accompanying the reaction $Rd_{ox} + e^- \rightleftharpoons Rd_{red}$. An Fe–S bond distance increase of 0.1 Å upon reduction is indicated. Factors relevant to the enthalpic structural barriers to electron transfer in Rd proteins and analogues are briefly discussed.

One of the principal goals of our research program concerning synthetic analogues[3,4] of the active sites of iron–sulfur proteins[5,6] is the preparation and full structural and electronic characterization of analogues corresponding to proteins in all of their physiologically significant oxidation levels. For 2-Fe ($[Fe_2S_2(S\text{-}Cys)_4]$) and 4-Fe ($[Fe_4S_4(S\text{-}Cys)_4]$) active sites and their analogues, in which thiolate ligands simulate terminal cysteinate coordination in the proteins, the following oxidation level equivalencies have been experimentally established.[7] $[Fe_2S_2(SR)_4]^{2-} \equiv$ 2-Fe Fd_{ox};[1,3,4] $[Fe_4S_4(SR)_4]^{2-} \equiv$ 4-,8-Fe Fd_{ox}, HP_{red};[3,4] $[Fe_4S_4(SR)_4]^{3-} \equiv$ 4-,8-Fe Fd_{red}, $HP_{s\text{-}red}$.[3,4] Binuclear dianions and tetranuclear dianions and trianions have been isolated, electronic structures investigated in some detail,[1,4,8] and precise structures of representative 4-Fe[9] and 2-Fe[10] species determined. The indicated oxidation level equivalencies are particularly useful in the 4-Fe case, inasmuch as the electronically delocalized nature of the Fe_4S_4 core prevents recognition of integral Fe(II,III) valence states by spectroscopic[8a] or diffraction methods.[6,9]

The third type of recognized active site ($[Fe(S\text{-}Cys)_4]$) in iron–sulfur redox proteins is found in the 1-Fe proteins, rubredoxins,[5,6,11] obtained from bacteria. The molecular weights of these proteins are typically about 6000; Rd from the aerobe *Pseudomonas oleovorans* has a molecular weight of 19 000 and can be obtained in a 1-Fe or 2-Fe form.[12] The latter appears to contain two noninteracting $[Fe(S\text{-}Cys)_4]$ sites similar to the single sites in the smaller proteins. The presence of only one iron atom per site renders an electronic description of the site somewhat simpler than for the 2-Fe and 4-Fe cases. Magnetic susceptibility[13] and a variety of spectroscopic results, including optical absorption,[11a,14,15] MCD,[11a,16] EPR,[17] and Mössbauer[13,18] data, have demonstrated that the two redox states of these proteins, Rd_{ox} and Rd_{red}, coupled by one-electron transfer at $E_0' \sim -0.04$ to -0.06 V,[12a,14a] contain Fe(III) and Fe(II), respectively. The results of many of the physical studies on Rd proteins are summarized elsewhere.[11a] The x-ray structural determination of *Clostridium pasteurianum* Rd_{ox} has progressed through a series of refinements,[6,19] with the latest published results obtained at 1.5-Å resolution. The active site structure is described as a severely distorted $Fe(III)\text{-}S_4$ tetrahedron with one unusually short (2.05 Å) Fe–S bond. Pronounced ligand field rhombicity has been detected by a number of spectroscopic measurements on both the oxidized and reduced forms.[11a]

Attainment of minimal analogues for the active sites of Rd proteins requires synthesis and characterization of tetrakis(thiolato)iron(II) and -(III) complexes, preferably derived from aliphatic ($-CH_2S^-$) ligands. Obligatory analogue properties include overall tetrahedral stereochemistry effected by the same ligand set in both oxidation levels and demonstrable interconversion between these levels, thereby defining the simple two-membered electron-transfer series

$$[Fe(SR)_4]^- \equiv Rd_{ox} \underset{-e^-}{\overset{+e^-}{\rightleftharpoons}} [Fe(SR)_4]^{2-} \equiv Rd_{red}$$

Discrete tetrahedral $Fe(II,III)\text{-}S_4$ complexes which are well

Table I. Summary of Crystal Data, Intensity Collection, and Refinement

	$[Fe(S_2\text{-}o\text{-xyl})_2]^-$	$[Fe(S_2\text{-}o\text{-xyl})_2]^{2-}$
Formula	$[N(C_2H_5)_4][Fe((SCH_2)_2C_6H_4)_2]$ $C_{24}H_{36}FeNS_4$	$Na[As(C_6H_5)_4][Fe((SCH_2)_2C_6H_4)_2]\cdot 2CH_3CN$ $C_{44}H_{42}AsFeN_2NaS_4$
Mol. wt	522.66	880.85
a, Å	13.413 (8)	13.67 (1)
b, Å	29.554 (17)	14.60 (1)
c, Å	13.448 (10)	11.59 (1)
α, deg		109.3 (1)
β, deg		105.6 (1)
γ, deg		71.6 (1)
V, Å^3	5331	2036
Z	8	2
d_{calcd}, g/cm^3	1.302	1.437
d_{obsd}, g/cm^3		1.39 (3)
Space group	C_{2v}^9-$Pn2_1a$	C_i^1-$P\bar{1}$
Crystal volume, mm^3	0.0853	0.171
Crystal shape	Truncated rod with faces {100}, {010}, {001}, (121), ($1\bar{2}\bar{1}$), ($1\bar{2}1$), ($0\bar{1}\bar{1}$), ($0\bar{1}1$)	Complex, bounded by ($\bar{2}11$), {110}, ($\bar{1}2\bar{2}$), ($0\bar{1}1$), ($0\bar{1}0$), ($11\bar{1}$).
Radiation	Mo (λ Kα_1 = 0.70930 Å) monochromatized from (002) face of mosaic graphite	Cu (λ Kα_1 = 1.540562 Å) prefiltered with 1 mil of Ni foil
Transmission factors	0.732–0.801	0.079–0.205
μ, cm^{-1}	8.77	61.7
Receiving aperture	2.5 mm wide by 4.0 mm high 32 cm from crystal	6 mm wide by 6 mm high 24 cm from crystal
Takeoff angle, deg	2.5	6.5
Scan speed	2° in 2θ/min	2° in 2θ/min
Scan range	0.95° below Kα_1 to 0.85° above Kα_2	1.4° below Kα_1 to 1.4° above Kα_2
Background counts	10 s	10 s
2θ limit, deg	55	92
Data collected	$h, k, l > 0$; $h, k, l < 0$ to 25°	$h \geq 0, \pm k, \pm l$
Data used in refinement	All 6941 observations, including Friedel pairs	2497 unique reflections having $F_o^2 > 3\sigma(F_o^2)$
p for calculation of $\sigma(F_o^2)$	0.03	0.05
Structure solution	MULTAN based on 214 E values	MULTAN based on 252 E values
Function minimized	$\Sigma w(F_o^2 - F_c^2)^2$	$\Sigma w(\lvert F_o\rvert - \lvert F_c\rvert)^2$
w	$1/\sigma^2(F_o^2)$	$4F_o^2/\sigma^2(F_o^2)$
No. of variables	372	208
$R(F^2)$	0.068 (includes $F_o^2 \leq 0$)	0.150 ($F_o^2 > 3\sigma(F_o^2)$)
$wR(F^2)$	0.105	0.210
$R(F)$, $F_o^2 > 3\sigma(F_o^2)$	0.045	0.087
$wR(F)$, $F_o^2 > 3\sigma(F_o^2)$	0.051	0.105
Error in observation of unit weight	1.78 e^2	3.05 e
Maximum electron density on final difference map, e$^-$/Å^3	0.3	1.1
No. of unobserved reflections	0	1029
No. with $\lvert F_o^2 - F_c^2\rvert > 5\sigma(F_o^2)$	0	3
Trends in minimized function	None	Worse at low 2θ values

characterized are not numerous. Among those which may be considered, to varying extents, as models of Rd_{red} sites are $Fe[(SPR_2)_2N]_2$,[20a] $Fe[(SPR_2)_2CH]_2$,[20b] $[Fe(Boc\text{-}Gly\text{-}(Cys\text{-}Gly\text{-}Gly)_3\text{-}Cys\text{-}Gly\text{-}NH_2)]^{2-}$,[21] ([iron(12-peptide)]$^{2-}$), bis(dithiosquarate)ferrate(II)[22] ([$Fe(dts)_2]^{2-}$), $[Fe(dts)(SPh)_2]^{2-}$,[23] and $[Fe(SPh)_4]^{2-}$.[23] The x-ray structure of $Fe[(SPMe_2)_2N]_2$ has been determined[24,25] and considered as a reasonable stereochemical representation of a Rd_{red} site. None of these Fe(II) complexes has as yet been shown to be oxidizable to the corresponding Fe(III) species. In order to provide $Rd_{ox,red}$ active site analogues with the obligatory properties, we have recently synthesized and characterized bis(*o*-xylyl-α,α'-dithiolato)ferrate(III) monoanion, $[Fe(S_2\text{-}o\text{-xyl})_2]^-$,[26] a Rd_{ox} analogue. Here we report full structural details for this complex and its reduced form, $[Fe(S_2\text{-}o\text{-xyl})_2]^{2-}$, a Rd_{red} analogue. Also described are certain physical properties of both complexes. These results complete the set of synthetic analogues of the three recognized types of active sites in low molecular weight iron–sulfur redox proteins, and allow the first assessment of Fe–S analogue stereochemical alterations pursuant to electron transfer.

Experimental Section

Preparation of Compounds. All manipulations were performed under a pure dinitrogen atmosphere and all solvents were carefully degassed prior to use. *o*-Xylyl-α,α'-dithiol was prepared as previously described[10] and distilled before use. Acetonitrile was purified by distillation from calcium hydride. Other solvents were the best commercial grades available and were not further purified. Bis(tetraethylammonium)tetrachlorometalate(II) salts of iron, cobalt, and nickel were obtained by published procedures;[27] the tetraphenylarsonium iron(II) salt was prepared by an analogous method. The syntheses of tetraethylammonium bis(*o*-xylyl-α,α'-dithiolato)ferrate(III), $(Et_4N)[Fe(S_2\text{-}o\text{-xyl})_2]$, and bis(tetraethylammonium) tris(*o*-xylyl-α,α'-dithiolato)diferrate(II), $(Et_4N)_2[Fe_2(S_2\text{-}o\text{-xyl})_3]$, have been described elsewhere.[26]

(a) Sodium Tetraphenylarsonium Bis(*o*-xylyl-α,α'-dithiolato)ferrate(II), $Na(Ph_4As)[Fe(S_2\text{-}o\text{-xyl})_2]$. To a suspension of *o*-xylyl-α,α'-dithiol (7.3 g, 43 mmol) and $(Ph_4As)_2(FeCl_4)$ (12 g, 13 mmol) in 100

Table II. Positional and Thermal Parameters for the Nongroup Atoms of $(Et_4N)[Fe(S_2\text{-}o\text{-}xyl)_2]$

ATOM	A X	Y	Z	B B11	B22	B33	B12	B13	B23
FE(1)	0.075041(64)	1/4	-0.481960(54)	47.14(57)	11.59(10)	48.92(45)	).67(21)	1.40(43)	-2.28(20)
FE(2)	0.054452(55)	-0.004656(36)	-0.056079(64)	45.23(45)	10.85(10)	78.64(60)	-3.02(19)	-3.55(45)	0.7122)
S(11)	0.10985(15)	0.219721(66)	-0.63276(11)	122.1(16)	17.23(25)	50.26(94)	14.21(56)	-8.0(10)	-5.26(42)
S(12)	0.10900(14)	0.202100(63)	-0.35565(11)	105.7(15)	16.26(24)	48.94(90)	3.39(49)	5.67(95)	2.35(39)
S(13)	-0.08904(12)	0.268465(57)	-0.48618(12)	61.4(10)	13.36(21)	79.0(11)	-2.25(39)	2.76(87)	-2.41(41)
S(14)	0.16674(11)	0.314167(59)	-0.46041(11)	48.83(89)	13.87(20)	71.0(10)	).46(36)	-0.30(79)	0.15(40)
S(21)	-0.09646(10)	-0.037708(61)	-0.08065(15)	44.62(88)	13.81(22)	124.8(16)	-3.49(37)	5.54(97)	-6.39(51)
S(22)	0.18110(10)	-0.053105(57)	-0.08348(12)	43.08(80)	12.00(19)	102.9(13)	-0.47(34)	-8.92(87)	0.94(44)
S(23)	0.05429(12)	0.022357(62)	0.10152(12)	72.7(11)	13.93(22)	70.2(11)	-4.59(42)	-1.80(92)	7.08(40)
S(24)	0.07304(10)	0.053567(56)	-0.16557(11)	57.91(89)	12.38(19)	57.94(91)	0.20(36)	-3.06(77)	-1.02(36)
N(1)	0.00271(30)	0.35370(14)	-0.17890(30)	44.7(27)	13.76(65)	48.5(27)	3.9(11)	-0.1(22)	-0.9(12)
N(2)	0.14716(30)	-0.39722(15)	-0.50586(32)	34.2(25)	14.10(66)	64.2(31)	5.2(11)	-2.0(23)	1.4(12)
C(11)	0.22710(48)	0.19057(20)	-0.61321(47)	84.0(50)	15.39(96)	90.7(51)	5.0(18)	29.2(41)	3.6(18)
C(12)	0.22522(46)	0.17502(24)	-0.39562(46)	67.1(46)	26.0(13)	83.1(50)	6.3(20)	-24.1(40)	-1.6(22)
C(13)	-0.08733(44)	0.31205(23)	-0.58496(41)	69.3(42)	20.3(11)	51.3(35)	3.0(18)	-15.0(31)	-0.1(17)
C(14)	0.11943(41)	0.34984(19)	-0.56292(40)	44.3(41)	14.98(88)	62.8(39)	-1.4(16)	18.6(33)	4.1(16)
C(21)	-0.07617(40)	-0.06555(20)	-0.20009(48)	41.0(39)	12.38(82)	97.1(49)	-4.4(15)	-32.0(37)	3.9(17)
C(22)	0.14410(40)	-0.08382(21)	-0.19650(45)	55.1(39)	17.45(95)	84.5(46)	-7.1(16)	5.5(35)	0.1(18)
C(23)	-0.04549(43)	0.06483(24)	0.08629(47)	55.0(41)	23.1(12)	73.4(43)	2.3(17)	10.3(34)	-4.2(19)
C(24)	-0.03186(45)	0.09133(20)	-0.12865(46)	75.9(45)	15.01(93)	75.8(47)	12.8(17)	-22.5(37)	-6.9(17)
C(1A)	0.05388(43)	0.38492(21)	-0.25049(45)	69.9(42)	17.17(94)	64.1(40)	4.5(17)	18.8(35)	6.8(18)
C(1B)	0.10933(48)	0.42406(22)	-0.20080(50)	82.5(51)	15.4(10)	142.3(69)	-6.9(20)	38.2(49)	-8.7(24)
C(1C)	-0.04163(42)	0.31686(20)	-0.24340(43)	64.7(40)	16.08(89)	66.3(40)	2.0(16)	1.6(33)	-8.0(17)
C(1D)	-0.09675(46)	0.27937(21)	-0.18669(55)	73.4(47)	15.09(99)	116.8(59)	-6.7(18)	6.6(43)	-2.8(21)
C(1E)	0.07671(44)	0.33371(23)	-0.10434(43)	58.6(39)	20.9(11)	65.5(41)	7.7(17)	-14.0(34)	2.4(18)
C(1F)	0.16163(45)	0.30762(23)	-0.15089(48)	57.3(42)	21.2(11)	105.4(54)	9.6(18)	-5.7(39)	9.4(22)
C(1G)	-0.07549(43)	0.37783(21)	-0.11694(42)	62.6(40)	17.27(98)	59.5(39)	5.9(17)	10.3(32)	-5.0(16)
C(1H)	-0.15411(44)	0.40185(23)	-0.17677(49)	59.9(43)	21.5(12)	104.4(56)	13.9(18)	-11.0(40)	-15.3(22)
C(2A)	0.07990(52)	-0.42306(24)	-0.57576(59)	83.2(53)	18.3(11)	111.2(62)	-7.2(20)	-41.8(47)	4.5(22)
C(2B)	0.13202(54)	-0.45729(23)	-0.64265(53)	104.8(59)	17.4(11)	110.7(61)	12.5(21)	-30.3(47)	-13.9(22)
C(2C)	0.21033(56)	-0.42861(27)	-0.44429(59)	96.2(56)	25.2(14)	121.1(65)	17.1(23)	-31.3(51)	4.2(27)
C(2D)	0.14286(69)	-0.45987(27)	-0.37459(59)	184.3(93)	24.7(15)	112.2(68)	-22.7(31)	-36.1(64)	26.7(27)
C(2E)	0.22208(52)	-0.36860(24)	-0.56337(52)	79.1(50)	19.2(11)	98.9(56)	-7.4(20)	8.8(44)	-2.0(22)
C(2F)	0.17432(63)	-0.33605(26)	-0.63584(51)	151.6(80)	22.9(13)	75.4(51)	17.7(28)	28.0(51)	7.6(22)
C(2G)	0.07968(55)	-0.36807(28)	-0.44249(55)	90.1(55)	27.4(14)	86.8(56)	19.1(23)	5.0(46)	-3.8(24)
C(2H)	0.13999(68)	-0.33970(27)	-0.36495(53)	148.3(85)	22.9(13)	74.4(53)	10.9(29)	-40.9(56)	-8.3(23)

[a] Estimated standard deviations in the least significant figure(s) are given in parentheses in this and all subsequent tables. [b] The form of the anisotropic thermal ellipsoid is: $\exp[-(B_{11}h^2 + B_{22}k^2 + B_{33}l^2 + 2B_{12}hk + 2B_{13}hl + 2B_{23}kl)]$. The quantities given in the table are the thermal coefficients $\times 10^4$.

ml of ethanol at 0 °C was added slowly with stirring 50 ml of a 1.73 M solution of sodium ethoxide in ethanol. The mixture was warmed to room temperature, sodium chloride was removed by filtration, and the rose-colored filtrate was concentrated in vacuo until crystallization began. After cooling to −20 °C, 6.0 g (52%) of orange, red, and black crystals were collected. Further volume reduction and cooling of the filtrate gave an additional 3.2 g of product, for a total yield of 80%. The crude product was recrystallized from acetonitrile initially at 50 °C, affording large, dark red crystals of the product, whose analysis is suggestive of a diacetonitrile solvate. Anal. Calcd for $C_{44}H_{42}AsFeN_2NaS_4$: C, 60.00; H, 4.81; As, 8.51; Fe, 6.34; N, 3.18; Na, 2.61; S, 14.56; formula weight 881. Found: C, 59.89; H, 4.89; As, 8.21; Fe, 5.92; N, 3.13; Na, 2.67; S, 13.91; formula weight 853 (from experimental density and crystal data, Table I). The composition of this material is further discussed in the text.

(b) Bis(tetraethylammonium) Bis(*o*-xylyl-α,α′-dithiolato)ferrate(II), $(Et_4N)_2[Fe(S_2\text{-}o\text{-}xyl)_2]$. To a suspension of *o*-xylyl-α,α′-dithiol (13 g, 77 mmol), $(Et_4N)_2(FeCl_4)$ (10 g, 22 mmol), and anhydrous Et_4NCl (11 g, 66 mmol) in 150 ml of ethanol at 0 °C was added slowly with stirring 100 ml of a 1.50 M solution of sodium ethoxide in ethanol. The mixture was warmed to room temperature, sodium chloride was removed by filtration, and the yellow filtrate was concentrated in vacuo to a thick light-brown oil. The oil was dissolved in excess acetonitrile at room temperature, the solution warmed to 50 °C, and concentrated until crystals began to form. Cooling to −20 °C produced 9.1 g (63%) of small light-orange crystals. Further concentration and cooling of the filtrate gave an additional 4.2 g of product, for a total yield of 92%. The product was purified by recrystallization from hot acetone/acetonitrile to give well-formed brownish-yellow crystals. Anal. Calcd for $C_{32}H_{56}FeN_2S_4$: C, 58.87; H, 8.66; Fe, 8.55; N, 4.29; S, 19.64. Found: C, 58.63; H, 8.51; Fe, 8.37; N, 4.21; S, 19.51.

Alternatively this compound may be prepared by reaction of $(Et_4N)_2[Fe_2(S_2\text{-}o\text{-}xyl)_3]$[26] with $(Et_4N)_2(S_2\text{-}o\text{-}xyl)$. The latter salt, generated in situ from the dithiol (1.6 g, 9.6 mmol), anhydrous Et_4NCl (3.2 g, 19 mmol), and sodium ethoxide (19 mmol) in 100 ml of ethanol, was filtered directly into a solution of 2.4 g (2.7 mmol) of $(Et_4N)_2[Fe_2(S_2\text{-}o\text{-}xyl)_3]$ in 75 ml of acetonitrile at room temperature. The resulting light yellow solution was treated as was the filtrate in the preceding preparation, affording 2.6 g (83%) of product, identical in all respects with the material obtained in that preparation.

(c) Bis(tetraphenylarsonium) Bis(*o*-xylyl-α,α′-dithiolato)ferrate(II), $(Ph_4As)_2[Fe(S_2\text{-}o\text{-}xyl)_2]$. In a manner analogous to a preceding prep-

Table III. Derived Parameters for the Rigid Group Atoms of $(Et_4N)[Fe(S_2\text{-}o\text{-}xyl)_2]$

ATOM	X	Y	Z	B, Å²	ATOM	X	Y	Z	B, Å²
C1R1	0.21222(32)	0.14393(11)	-0.56855(29)	4.76(12)	C1R3	-0.03291(25)	-0.11241(093)	-0.18366(27)	3.93(11)
C2R1	0.19785(31)	0.10780(15)	-0.63333(20)	6.29(15)	C2R3	-0.10007(18)	-0.14783(12)	-0.17091(26)	4.38(11)
C3R1	0.18223(34)	0.06449(12)	-0.59582(30)	6.21(15)	C3R3	-0.06518(25)	-0.19134(10)	-0.15214(29)	5.08(13)
C4R1	0.18099(36)	0.05731(11)	-0.49357(32)	6.99(17)	C4R3	0.03687(28)	-0.19944(096)	-0.14612(31)	5.33(13)
C5R1	0.19537(33)	0.09344(15)	-0.42875(21)	6.47(16)	C5R3	0.10403(19)	-0.16402(13)	-0.15887(27)	4.78(12)
C6R1	0.21098(32)	0.13675(12)	-0.46626(26)	4.72(12)	C6R3	0.06914(23)	-0.12051(11)	-0.17764(26)	4.11(11)
C1R2	-0.06860(28)	0.35814(10)	-0.54530(27)	4.06(11)	C1R4	-0.00625(28)	0.11024(10)	0.05320(26)	4.12(11)
C2R2	-0.15056(21)	0.38438(14)	-0.51885(29)	5.55(14)	C2R4	0.02431(30)	0.14016(14)	0.12703(19)	5.09(13)
C3R2	-0.13666(27)	0.42823(13)	-0.48383(30)	6.18(15)	C3R4	0.05932(32)	0.18292(13)	0.10138(26)	5.88(15)
C4R2	-0.04081(33)	0.44585(10)	-0.47526(31)	6.29(15)	C4R4	0.06376(31)	0.19576(10)	0.00189(30)	6.09(15)
C5R2	0.04115(24)	0.41961(13)	-0.50170(30)	5.04(13)	C5R4	0.03320(29)	0.16583(13)	-0.07195(20)	5.19(13)
C6R2	0.02725(23)	0.37575(12)	-0.53672(27)	4.03(11)	C6R4	-0.00181(28)	0.12307(12)	-0.04630(23)	4.11(11)

RIGID GROUP PARAMETERS

GROUP	X_C, Å	Y_C	Z_C	DELTA, rad	EPSILON	ETA
RING1	0.19661(20)	0.10062(97)	-0.53104(20)	-0.1697(27)	-2.9888(24)	-1.5848(24)
RING2	-0.05471(21)	0.40199(92)	-0.51028(17)	-2.7265(23)	2.7915(23)	-0.0883(25)
RING3	0.00198(18)	-0.15592(87)	-0.16489(15)	-0.1835(20)	2.9648(24)	-3.0825(21)
RING4	0.02876(19)	0.15299(91)	0.02754(19)	2.7530(25)	2.8694(21)	-1.5072(23)

[a] X_C, Y_C, and Z_C are the fractional coordinates of the origin of the rigid group. [b] The rigid group orientation angles delta, epsilon, and eta (radians) have been defined previously: S. J. La Placa and J. A. Ibers, *Acta Crystallogr.*, 18, 511 (1965).

aration, 14 mmol of dithiol, 3.7 mmol of $(Ph_4As)_2(FeCl_4)$, and 11 mmol of anhydrous Ph_4AsCl in 75 ml of ethanol were combined with 50 ml of a 0.52 M solution of sodium ethoxide in ethanol. The thick gum obtained after concentration of the filtrate was extracted with 75 ml of acetonitrile at 50 °C, a small amount of green residue removed by filtration, and the filtrate slowly cooled to room temperature. The resulting red-black crystals were collected, washed with acetone until the washings were very faint yellow, and then washed with 5 ml of cool acetonitrile, affording 0.9 g (20%) of crystals. Anal. Calcd for $C_{64}H_{56}As_2FeS_4$: C, 66.32; H, 4.87; Fe, 4.82; S, 11.07. Found: C, 66.02; H, 4.98; Fe, 4.80; S, 11.13.

(d) Bis(tetraethylammonium) Bis(*o*-xylyl-α,α′-dithiolato)cobaltate(II), $(Et_4N)_2[Co(S_2\text{-}o\text{-}xyl)_2]$. This preparation followed closely that of the iron(II) analogue, and employed $(Et_4N)_2(CoCl_4)$ (21 mmol), dithiol (74 mmol), Et_4NCl (63 mmol), and 100 ml of a 1.47 M solution of sodium ethoxide in ethanol. The deep blue filtrate was concentrated to dryness in vacuo, the residue was redissolved in acetonitrile at room temperature, and the solution filtered. This solution was warmed to 40 °C and concentrated until crystallization began. Two crops of product were obtained as for the iron(II) analogue, resulting in a total of 13 g (95%). The compound was further purified by recrystallization from acetonitrile/acetone initially at 55 °C, giving aqua-blue crystals. Anal. Calcd for $C_{32}H_{56}CoN_2S_4$: C, 58.59; H, 8.60; N, 4.27. Found: C, 58.45; H, 8.64; N, 4.27.

(e) Bis(tetraethylammonium) Tris(*o*-xylyl-α,α′-dithiolato)dinickelate(II), $(Et_4N)_2[Ni_2(S_2\text{-}o\text{-}xyl)_3]$. The preceding preparation was followed, using $(Et_4N)_2(NiCl_4)$ (19 mmol), dithiol (65 mmol), Et_4NCl (56 mmol), and 100 ml of a 1.3 M sodium ethoxide solution. The reaction mixture was concentrated to produce a dark red gum. This material was extracted with 200 ml of acetonitrile at 60 °C, the extract filtered, and the filtrate cooled to give 2.1 g of brownish-purple crystals. A second extraction afforded an additional 1.4 g, for a total yield of 43%. Recrystallization of this material from hot acetonitrile yielded the pure product as black crystals. Anal. Calcd for $C_{40}H_{64}N_2Ni_2S_6$: C, 54.42; H, 7.32; N, 3.17. Found: C, 54.64; H, 7.39; N, 3.22.

Crystal Structure Determinations. Pertinent details on crystal data, collection of intensity data, and course of the refinements are given in Table I. Particulars on methods employed, computer programs used, sources of atomic scattering factors, and related matters have been given previously for related structures.[9]

(a) $(Et_4N)[Fe(S_2\text{-}o\text{-}xyl)_2]$. Refinement of this structure presented no problems other than those associated with the unexpectedly large number of independent atoms in the asymmetric unit arising from the presence of two independent cations and anions in the noncentrosymmetric space group $Pn2_1a$, rather than the expected single independent cation and anion in the more common centrosymmetric space group *Pnma*. The refinement model included anisotropic thermal parameters for all nongroup, nonhydrogen atoms. The four independent phenyl rings were treated as rigid groups[28] of D_{6h} symmetry, C–C = 1.392 Å, with individual isotropic thermal parameters. The sense of the polar axis was fixed on the basis of comparison of the Friedel pairs of reflections that would be equivalent in the absence of anomalous scattering. On a difference Fourier map, computed after anisotropic refinement, the positions of all hydrogen atoms could be discerned. These hydrogen atom positions on the methyl, methylene, and phenyl carbon atoms were idealized, utilizing a C–H distance of 0.95 Å and an isotropic thermal parameter for a given H atom that was 1 Å² greater than the equivalent isotropic thermal parameter of the C atom to which it is attached. The full-matrix least-squares refinements, involving 372 variables and 6941 observations, were carried out by remote hookup to the CDC7600 computer at Lawrence Berkeley laboratory. Final values of the parameters are given in Tables II and III. Idealized positions of the hydrogen atoms are given in Table IV and the root-mean-square amplitudes of vibration in Table V. In Table VI are presented the values of F_o^2 and F_c^2 for the 6941 observations.[29]

(b) $Na(Ph_4As)[Fe(S_2\text{-}o\text{-}xyl)_2]$ Acetonitrile Solvate. Data collection and refinement of this structure were less satisfactory. A number of crystals was examined photographically and all were found to be highly mosaic and hence unsuitable for a high-precision structure determination. Since no more suitable crystals involving other cations were available at this stage of the research and because of the importance of a stereochemical comparison of the Fe(III)–S_4 and Fe(II)–S_4 units, the structure determination was pursued. The high mosaicity of the chosen crystal with the concomitant necessity for wide scans and a closely positioned counter forced the use of Cu rather than Mo radiation in order to avoid overlapping reflections. The Bragg peaks contained considerable structure, which made accurate centering of the crystal difficult.

With the exception of the location of one of the solvate molecules, the refinement of the structure proceeded smoothly. The other solvate

Table VII. Positional and Thermal Parameters for the Nongroup Atoms of $Na(Ph_4As)[Fe(S_2\text{-}o\text{-}xyl)_2]$ Acetonitrile Solvate

ATOM	A X	Y	Z	B B11	B22	B33	B12	B13	B23
AS	0.16005(13)	0.06252(12)	0.41754(16)	46.6(13)	59.2(13)	89.1(20)	-3.16(97)	-5.4(12)	-6.3(12)
FE	-0.35216(18)	0.29984(18)	-0.04062(22)	51.4(19)	61.4(19)	94.5(29)	3.8(14)	0.0(18)	2.1(18)
S(1)	-0.53195(30)	0.38375(29)	-0.08657(38)	57.0(32)	57.2(30)	109.3(49)	1.2(24)	-5.4(31)	2.3(30)
S(2)	-0.33543(30)	0.12793(30)	-0.10569(42)	54.6(32)	62.5(31)	140.2(55)	2.5(25)	-11.3(33)	6.7(32)
S(3)	-0.29998(33)	0.33292(33)	0.17621(39)	72.3(35)	83.8(35)	102.6(49)	-12.9(28)	-8.2(32)	12.6(33)
S(4)	-0.25809(33)	0.35764(33)	-0.13569(39)	73.6(36)	84.6(36)	106.2(51)	-17.6(28)	13.6(34)	-2.9(33)
NA	0.46776(55)	0.49487(54)	0.17643(63)	111.5(64)	115.0(63)	134.8(86)	-26.6(50)	12.3(59)	23.8(58)
C(1)	-0.6054(13)	0.2987(12)	-0.2081(14)	80.(15)	78.(13)	92.(18)	-14.(11)	-27.(13)	-12.(12)
C(2)	-0.4509(11)	0.1023(12)	-0.2225(14)	58.(12)	90.(15)	78.(18)	-10.(10)	-6.(11)	3.(13)
C(3)	-0.2388(12)	0.4366(12)	0.2251(15)	86.(14)	69.(13)	120.(21)	-17.(11)	4.(14)	1.(13)
C(4)	-0.2013(12)	0.4559(11)	-0.0132(15)	92.(15)	61.(12)	120.(20)	-14.(10)	13.(13)	3.(12)
X	0.4547(11)	0.3228(11)	0.1773(12)	205.(15)	232.(14)	155.(18)	-96.(11)	-13.(13)	96.(13)
SN(2)	0.5412(16)	0.5512(17)	0.4014(19)	139.(22)	174.(21)	163.(28)	-16.(17)	20.(18)	19.(19)
SC(2)	0.6101(21)	0.5333(16)	0.4791(23)	141.(29)	94.(17)	189.(36)	-33.(18)	64.(26)	-12.(20)
SME(2)	0.6998(16)	0.5053(20)	0.5799(20)	143.(20)	274.(33)	227.(30)	-85.(20)	-107.(21)	143.(26)

[a] Estimated standard deviations in the least significant figure(s) are given in parentheses in this and all subsequent tables. [b] The form of the anisotropic thermal ellipsoid is: $\exp[-(B_{11}h^2 + B_{22}k^2 + B_{33}l^2 + 2B_{12}hk + 2B_{13}hl + 2B_{23}kl)]$. The quantities given in the table are the thermal coefficients $\times 10^4$.

entity was located without difficulty and refinement led to a reasonable geometry for an acetonitrile molecule. The troublesome solvate molecule could not be located in its entirety. An atom, denoted X, was located at about the same distance from the Na atom as the N atom of the satisfactory acetonitrile molecule, in such a position as to complete a distorted octahedral environment about the Na atom. Atom X, as well as the three nonhydrogen atoms of the well-defined acetonitrile molecule, all displayed electron densities in excess of 2.1 e/Å^3 on earlier difference Fourier maps. After anisotropic refinement of all nonhydrogen, nonring atoms (including X and the well-defined acetonitrile molecule) an ensuing difference Fourier map was searched closely for other fragments of the troublesome solvate molecule. The one possibly significant feature on this map is a peak Y of height 1.1 e/Å^3 located 1.54 Å from X. Down to a height of 0.3 e/Å^3, which is certainly in the noise region, there were no other features on the map that are in the vicinity of atoms X or Y. There are several possible explanations for our difficulties with one of the solvate molecules. (1) The molecule is badly disordered. (2) Atom Y is a composite peak of the CCH_3 portion of an assumed acetonitrile molecule. (3) The molecular species, of which atom X is a part, is not acetonitrile. Explanation 1 seems unlikely in view of the absence of electron density about atom X and atom Y and because of the steric constraints imposed in the cell. Explanation 2 seems unlikely in view of the successful refinement of the other acetonitrile molecule. Explanation 3 can neither be supported nor rejected. The analytical data suggest but do not require the presence of two acetonitrile molecules per Fe atom in the bulk sample (vide infra). It is possible that the crystal chosen for data collection is not representative of the bulk sample. In view of the preparative conditions the ill-defined solvate molecule might be ethanol. But if this is the case, then X is an O atom, Y is the α-C atom, and the methyl group must be disordered. Water is a remote possibility in view of the anhydrous nature of solvents and compounds used in synthesis. If a water molecule were present, then X is an O atom and Y, which is near to the noise level of the difference Fourier map, must be an artifact. In view of the impossibility of resolving this problem with the present data set, the final refinement model involved the assignment of X as an O atom and the neglect of the Y atom. In the final refinement the nonhydrogen, nongroup atoms were refined anisotropically, the six phenyl rings (rings 1 and 2 of the anion and rings 3 through 6 of the Ph_4As^+ cation) were refined as described above. The positions of 36 H atoms (eight on the methylene groups, eight on the phenyl rings of the anion, and 20 on the phenyl rings of Ph_4As^+) were idealized and added as fixed contributions. No attempt was made to locate the H atoms on the CH_3 group of the ordered acetonitrile molecule. Final values of the parameters are given in Tables VII and VIII. Idealized positions for the H atoms may be found in Table IV and the root-mean-square amplitudes of vibration in Table V. Values of $10|F_o|$ and $10|F_c|$ are given in Table IX[29] for those reflections used in the refinement.

Other Physical Measurements. Mössbauer measurements were made from 1.4 K to room temperature with a constant acceleration spectrometer. The source (^{57}Co in Rh) was located in the cryostat and held at the same temperature as the absorber. Measurements were also made with the absorber in external magnetic fields up to 80 kOe with a superconducting magnet operating in a longitudinal configuration. Magnetic susceptibility measurements were carried out with a Superconducting Technology, Inc. susceptometer using $HgCo(NCS)_4$ as the calibrant. A Princeton Applied Research Model 170 electrochemistry system was employed for polarographic and cyclic voltammetric determinations. Solutions were $\sim 10^{-3}$ M in sample and 0.05 M in $(n\text{-}Pr_4N)(ClO_4)$ or $(n\text{-}Pr_4N)(PF_6)$ as supporting electrolyte. Potentials were determined at 25 °C vs. a saturated calomel electrode (SCE) as reference. Electronic spectra were recorded on a Cary Model 14 or 17 spectrophotometer.

Results and Discussion

Synthesis of Fe(II,III)–S_4 Complexes. Other than [iron(12-peptide)]$^{2-}$ (generated in solution[21]) and $[Fe(SPh)_4]^{2-}$ (isolated[23] during the course of this work), both of which have tetrahedral stereochemistry, previous investigations of the reactions of Fe(II,III) with thiolate ligands[30] have yielded few isolated complexes. Aqueous reactions of Fe(II) with cysteinate and mercaptoacetate yielded solids which are apparently octahedral polymers,[31] such as has been established for $Fe(S\text{-}CH_2CO_2)\cdot H_2O$.[32] The properties of these compounds or Fe(II) species produced in solution in various investigations are not suggestive of the Rd_{red} chromophore. Having previously demonstrated that *o*-xylyldithiolate affords near-tetrahedral stereochemistry in the 2-Fe(III) analogue $[Fe_2S_2(S_2\text{-}o\text{-}xyl)_2]^{2-}$,[10] this ligand was utilized in the synthesis of Fe(II,III) Rd analogues. Its choice in past and present work has been based on its S···S bite distance flexibility, which facilitates formation of tetrahedral angles with retention of normal high-spin Fe–S distances, i.e., in its seven-membered chelate ring no significant angular or distance constraints upon coordination stereochemistry are evident. At least with Fe(III), a less flexible ligand such as 1,2-ethanedithiolate is not suitable and a nontetrahedral binuclear complex, $[Fe_2(edt)_4]^{2-}$, results.[33,34] Some additional indication that flexible chelating dithiols $(HS(CH_2)_{4\text{-}6}SH)$ can form tetrahedral Fe(III) species is afforded by absorption spectral studies in aqueous alkaline

Table VIII. Derived Parameters for the Rigid Group Atoms of $Na(Ph_4As)[Fe(S_2\text{-}o\text{-}xyl)_2]$ Acetonitrile Solvate

ATOM	X	Y	Z	B, Å^2	ATOM	X	Y	Z	B, Å^2
C1R1	-0.62194(82)	0.21973(68)	-0.16728(96)	4.53(34)	C1R4	0.09006(79)	0.17328(65)	0.53160(88)	4.60(34)
C2R1	-0.71368(72)	0.23891(65)	-0.1235(10)	5.66(39)	C2R4	0.00398(86)	0.16688(67)	0.5681(10)	6.59(42)
C3R1	-0.73176(69)	0.16664(88)	-0.0836(10)	6.53(44)	C3R4	-0.05156(72)	0.25009(90)	0.6465(11)	7.01(46)
C4R1	-0.65810(91)	0.07519(75)	-0.0874(11)	6.88(46)	C4R4	-0.02101(84)	0.33971(71)	0.68829(95)	6.27(43)
C5R1	-0.56637(78)	0.05601(61)	-0.1312(11)	5.95(40)	C5R4	0.06507(90)	0.34611(63)	0.65181(10)	6.11(42)
C6R1	-0.54829(64)	0.12828(79)	-0.17117(96)	4.35(35)	C6R4	0.12060(71)	0.26290(82)	0.5734(10)	5.88(38)
C1R2	-0.13225(65)	0.41108(79)	0.1943(10)	4.63(34)	C1R5	0.05916(67)	0.02811(74)	0.27182(75)	4.19(34)
C2R2	-0.04765(91)	0.38162(86)	0.28391(81)	6.30(43)	C2R5	0.06627(68)	-0.07059(63)	0.20045(94)	4.99(36)
C3R2	0.05430(74)	0.35794(85)	0.26356(97)	6.50(42)	C3R5	-0.01024(85)	-0.09308(57)	0.09604(90)	5.37(38)
C4R2	0.07163(65)	0.36372(88)	0.1536(11)	7.22(45)	C4R5	-0.09385(71)	-0.01687(81)	0.06300(79)	5.64(39)
C5R2	-0.01297(92)	0.39318(88)	0.06390(87)	6.72(45)	C5R5	-0.10096(66)	0.08183(68)	0.13437(95)	5.71(39)
C6R2	-0.11491(75)	0.41685(77)	0.08425(87)	4.48(35)	C6R5	-0.02446(79)	0.10431(54)	0.23878(87)	5.04(36)
C1R3	0.26275(68)	0.10472(69)	0.38438(95)	3.91(32)	C1R6	0.22643(77)	-0.04791(62)	0.48471(98)	4.69(34)
C2R3	0.24481(63)	0.13816(75)	0.27942(83)	4.91(35)	C2R6	0.21651(82)	-0.04535(67)	0.60216(93)	5.90(42)
C3R3	0.31865(86)	0.17744(78)	0.26210(83)	5.79(40)	C3R6	0.26267(92)	-0.12965(89)	0.64680(78)	6.79(44)
C4R3	0.41043(74)	0.18328(78)	0.3497(11)	6.02(40)	C4R6	0.31875(83)	-0.21652(69)	0.5740(10)	6.28(40)
C5R3	0.42836(64)	0.14983(82)	0.45470(91)	6.34(42)	C5R6	0.32867(76)	-0.21908(62)	0.45654(95)	5.39(37)
C6R3	0.35452(81)	0.11055(77)	0.47202(77)	5.32(38)	C6R6	0.28251(82)	-0.13477(79)	0.41190(75)	4.89(36)

RIGID GROUP PARAMETERS

GROUP	X_C	Y_C	Z_C	DELTA	EPSILON	ETA
RING 1	-0.64002(55)	0.14746(54)	-0.12736(62)	1.2416(67)	-2.7510(66)	-0.3821(70)
RING 2	-0.03031(60)	0.38740(48)	0.17390(70)	-1.1115(96)	2.3519(67)	-2.2238(96)
RING 3	0.33659(52)	0.14400(45)	0.36706(65)	1.1241(94)	2.2700(63)	2.7205(95)
RING 4	0.03452(55)	0.25650(55)	0.60995(64)	2.4733(67)	-3.0497(66)	-2.3461(64)
RING 5	-0.01735(52)	0.00562(52)	0.16741(61)	-2.6207(62)	2.8744(59)	2.3458(64)
RING 6	0.27259(51)	-0.13221(54)	0.52935(67)	1.237(18)	-1.9493(63)	-0.825(18)

solution,[35] which reveal chromophores absorbing near the Rd_{ox} maxima of ~490 and ~380 nm.[11a,14] However, these species were not isolated or further characterized, nor were complexes of cysteinate and related monocysteinyl peptide ligands,[36] whose spectra also show some resemblance to Rd_{ox}.

As indicated in the preparative scheme (1) below and

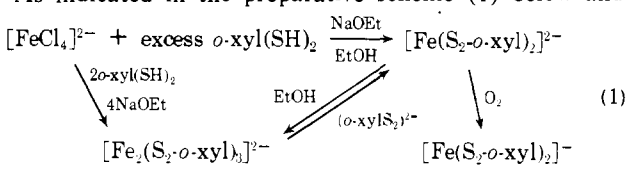

(1)

demonstrated by the structural results which follow, *o*-xylyl dithiolate affords discrete tetrahedral complexes of both Fe(II) and Fe(III). Of the synthetic procedures explored the use of quaternary salts of tetrachloroferrate(II) as the iron source and anhydrous ethanol as the reaction medium has led to the cleanest reaction systems. Reaction of $[FeCl_4]^{2-}$ with *excess* *o*-xyl$(SH)_2$ (ca. 3.5:1 mol ratio) yields the desired $[Fe(S_2\text{-}o\text{-}xyl)_2]^{2-}$, isolated as three different salts whose colors (brown-yellow to red-black) appear to depend on the cation and the presence of solvate molecules. These salts when finely crushed have similar light orange to yellow colors and all give the same solution absorption spectrum (vide infra), indicative of the presence of Fe(II) only. The use of 2:1 ligand/metal stoichiometry led, unexpectedly, to the formation of $[Fe_2(S_2\text{-}o\text{-}xyl)_3]^{2-}$,[26] hereafter considered as a binuclear dianion on the basis of analytical data only. This complex can be converted to the Fe(II) monomer upon treatment with excess thiol, and the monomer reconverted to $[Fe_2(S_2\text{-}o\text{-}xyl)_3]^{2-}$ in ethanol. In the latter case 2.0 mmol of the Et_4N^+ salt was dissolved in 50 ml of absolute ethanol at room temperature. An immediate light yellow to red color change was observed and after ~2 h 70% of the iron was recovered in the form of $(Et_4N)_2[Fe_2(S_2\text{-}o\text{-}xyl)_3]$, isolated after cooling the solution to −20 °C. Spontaneous conversion to the binuclear dianion does not occur in aprotic solvents such as DMF, Me_2SO, and acetonitrile. Controlled aerial oxidation of the isolated $[Fe(S_2\text{-}o\text{-}xyl)_2]^{2-}$ anion in solution or, more conveniently for preparative purposes, of the initial reaction filtrate containing this complex, affords $[Fe(S_2\text{-}o\text{-}xyl)_2]^-$, readily isolated as its black Et_4N^+ salt.[26]

Structural Descriptions. The crystal structures of $(Et_4N)[Fe(S_2\text{-}o\text{-}xyl)_2]$ and $Na(Ph_4As)[Fe(S_2\text{-}o\text{-}xyl)_2]$ acetonitrile solvate have been determined. Crystal data are collected in Table I. Metrical data for anions and cations of both compounds are presented in Tables X–XII.

(a) $(Et_4N)[Fe(S_2\text{-}o\text{-}xyl)_2]$. The crystal structure of this compound consists of well-separated cations and anions. A stereoview of the unit cell is presented in Figure 1. Two independent cations and anions are present per unit cell. The Et_4N^+ cations have their expected geometries (Table XI). The root-mean-square amplitudes of vibration (Table V) suggest some excessive thermal motion of some of the β-C atoms of one cation. Any disorder in these groups is very minor, as judged by the essentially featureless final difference Fourier map. The N–C distances average 1.514 (10) Å and the C–C distances 1.535 (31) Å, where the standard deviations in parentheses are of a single observation as estimated on the assumption that all observations are from the same population. That the standard

Table X. Comparison of Fe–S_4 Geometries in $[Fe(S_2\text{-}o\text{-xyl})_2]^-$ and $[Fe(S_2\text{-}o\text{-xyl})_2]^{2-}$

	Fe(III) anion 1	Fe(III) anion 2	Fe(II)
	Distance, Å		
Fe–S(1)	2.265 (2)	2.272 (2)	2.378 (5)
Fe–S(2)	2.258 (2)	2.252 (2)	2.324 (5)
Fe–S(3)	2.268 (2)	2.265 (2)	2.347 (5)
Fe–S(4)	2.279 (2)	2.278 (2)	2.376 (6)
S(1)···S(2)	3.763 (3)	3.751 (3)	3.830 (7)
S(3)···S(4)	3.704 (3)	3.717 (3)	3.955 (7)
S(1)···S(3)	3.617 (3)	3.639 (3)	3.834 (7)
S(1)···S(4)	3.708 (3)	3.708 (3)	3.819 (7)
S(2)···S(3)	3.740 (3)	3.749 (3)	3.669 (7)
S(2)···S(4)	3.682 (3)	3.641 (3)	3.961 (7)
S(1)–C(1)	1.812 (6)	1.825 (7)	1.844 (15)
S(2)–C(2)	1.833 (6)	1.839 (6)	1.831 (14)
S(3)–C(3)	1.851 (6)	1.846 (6)	1.813 (16)
S(4)–C(4)	1.848 (6)	1.863 (6)	1.853 (15)
C(1)–C1R(1,3)[a]	1.517 (7)	1.518 (7)	1.479 (25)
C(2)–C6R(1,3)	1.489 (8)	1.500 (7)	1.492 (19)
C(3)–C1R(2,4)	1.484 (7)	1.509 (8)	1.496 (20)
C(4)–C6R(2,4)	1.497 (7)	1.506 (7)	1.510 (18)
	Angle, deg		
S(1)–Fe–S(2)	112.60 (8)	112.02 (8)	109.1 (2)
S(1)–Fe–S(3)	105.82 (7)	106.67 (7)	108.5 (2)
S(1)–Fe–S(4)	109.35 (7)	109.16 (7)	106.9 (2)
S(2)–Fe–S(3)	111.44 (7)	112.20 (7)	103.5 (2)
S(2)–Fe–S(4)	108.49 (7)	106.97 (7)	114.9 (2)
S(3)–Fe–S(4)	109.07 (7)	109.80 (7)	113.8 (2)
Fe–S(1)–C(1)	103.7 (2)	100.9 (2)	110.6 (5)
Fe–S(2)–C(2)	103.0 (2)	104.2 (2)	108.7 (6)
Fe–S(3)–C(3)	100.0 (2)	97.8 (2)	106.3 (6)
Fe–S(4)–C(4)	101.2 (2)	101.4 (2)	107.1 (6)
S(1)–C(1)–C1R(1,3)	112.0 (4)	109.9 (4)	114.8 (10)
S(2)–C(2)–C6R(1,3)	114.2 (4)	113.5 (4)	114.5 (9)
S(3)–C(3)–C1R(2,4)	112.5 (4)	112.6 (4)	115.2 (9)
S(4)–C(4)–C6R(2,4)	113.6 (3)	111.5 (4)	114.1 (10)
	Dihedral Angle, deg		
Fe–S(1)–S(2) Fe–S(3)–S(4)	92.3	92.7	94.3
Fe–S(1)–S(2) C(1)–C(2)–S(1)–S(2)	39.8	45.3	20.0
Fe–S(3)–S(4) C(3)–C(4)–S(3)–S(4)	53.8	54.7	21.4
C(1)–C(2)–S(1)–S(2) C(1)–C(2)–R(1,3)	71	72	68
C(3)–C(4)–S(3)–S(4) C(3)–C(4)–R(2,4)	69	71	67

[a] The first ring number refers to Fe(III) anion 1 and to Fe(II); the second ring number refers to Fe(III) anion 2.

Table XI. Cation Geometries in $(Et_4N)[Fe(S_2\text{-}o\text{-xyl})_2]$

	Cation 1	Cation 2
	Distance, Å	
N–C(A)	1.500 (6)	1.510 (8)
N–C(C)	1.514 (6)	1.505 (7)
N–C(E)	1.530 (6)	1.524 (7)
N–C(G)	1.518 (6)	1.511 (8)
C(A)–C(B)	1.530 (8)	1.524 (9)
C(C)–C(D)	1.535 (8)	1.597 (10)
C(E)–C(F)	1.511 (8)	1.512 (9)
C(G)–C(H)	1.505 (8)	1.565 (10)
	Angle, deg	
C(A)–N–C(C)	104.7 (4)	111.5 (5)
C(A)–N–C(E)	111.2 (4)	111.0 (5)
C(A)–N–C(G)	112.3 (4)	106.3 (5)
C(C)–N–C(E)	110.7 (4)	104.5 (5)
C(C)–N–C(G)	112.4 (4)	112.3 (5)
C(E)–N–C(G)	105.7 (4)	111.3 (5)
N–C(A)–C(B)	114.0 (5)	115.4 (6)
N–C(C)–C(D)	115.1 (5)	111.1 (6)
N–C(E)–C(F)	114.5 (5)	113.6 (6)
N–C(G)–C(H)	114.4 (5)	111.8 (6)

Table XII. Other Distances (Å) and Angles (deg) in $Na(Ph_4As)$-$[Fe(S_2\text{-}o\text{-xyl})_2]$ Acetonitrile Solvate

As–C1R3	1.868 (12)	SN(2)–Na–S(1)′	99.8 (6)
As–C1R4	1.890 (9)	SN(2)–Na–S(1)″	157.2 (6)
As–C1R5	1.905 (8)	SN(2)–Na–S(4)″	105.4 (5)
As–C1R6	1.886 (10)	SN(2)–Na–S(3)′	82.1 (5)
Na···SN(2)	2.49 (2)	X–Na–S(1)′	152.5 (4)
Na···X	2.58 (2)	X–Na–S(1)″	78.9 (4)
Na···S(1)′[a]	2.77 (1)	X–Na–S(4)″	114.0 (4)
Na···S(1)″	2.94 (1)	X–Na–S(3)′	69.5 (4)
Na···S(4)″	3.02 (1)	S(1)′–Na–S(1)″	77.2 (2)
Na···S(3)′	3.31 (1)	S(1)′–Na–S(4)″	82.3 (2)
SN(2)–SC(2)	1.14 (3)	S(1)′–Na–S(3)′	91.3 (2)
SC(2)–SMe(2)	1.51 (3)	S(1)″–Na–S(4)″	96.7 (2)
C1R3–As–C1R4	106.3 (5)	S(1)″–Na–S(3)′	75.4 (2)
C1R3–As–C1R5	111.6 (5)	S(3)′–Na–S(4)″	170.8 (3)
C1R3–As–C1R6	108.5 (5)	SN(2)–SC(2)–SMe(2)	177 (3)
C1R4–As–C1R5	107.8 (4)		
C1R4–As–C1R6	111.9 (5)		
C1R5–As–C1R6	110.7 (4)		
SN(2)–Na–X	96.9 (7)		

[a] Primed atoms are at $\bar{x}$, $1-y$, $\bar{z}$; doubly primed atoms are at $1+x, y, z$.

deviation of the N–C distances estimated in this way is essentially that estimated for an individual N–C distance from the inverse matrix (0.008 Å) implies that these latter estimates are reasonable.

Stereoviews of the two independent anions in the cell are shown in Figure 2A, B. These anions are virtually identical, as can be seen from the stereoviews and the bond distance and angle data in Table X, and possess slightly distorted tetrahedral Fe(III)–S_4 coordination units which are depicted in Figure 3A, B. Inasmuch as the stereochemistry of $[Fe(S_2\text{-}o\text{-xyl})_2]^-$ has been discussed previously,[26] here considerations are restricted to a summary of its more important structural features: (i) ranges and mean values of Fe–S distances and S–Fe–S angles (both anions) are 2.252 (2)–2.279 (2), 2.267 (3) Å, and 105.82 (7)–112.60 (8), 109.5 (7)°, respectively; (ii) mean values of dihedral angles between FeS_2 planes (both anions) are 92.5°; (iii) from i and ii the Fe(III)–S_4 unit approaches T_d microsymmetry, but its precise symmetry is no higher than rhombic; (iv) the anions are dissymmetric[37a] owing to the nonplanar chair-type conformations of the chelate rings (Figure 2), in which acute FeS_2–C_2S_2 and C_2S_2–C_2Ph dihedral angles (both anions) occur in the ranges 40.0–54.7° and 69–72°, respectively; (v) the mean $\overline{S\cdots S}$ bite distance and S–Fe–S bite angle (both anions) of 3.734 Å and 110.9°, respectively, compare closely with the corresponding values (3.690 Å, 106.4°) in $[Fe_2S_2(S_2\text{-}o\text{-xyl})_2]^{2-}$;[10] (vi) the mean Fe–S distance of 2.267 Å together with the corresponding Fe–SR distances in $[Fe_2S_2(S_2\text{-}o\text{-xyl})_2]^{2-}$ (2.305 Å) and $[Fe_2S_2(SC_6H_4\text{-}p\text{-Me})_4]^{2-}$ (2.312 Å)[10] define a range of 2.27–2.31 Å for tetrahedral Fe(III)–thiolate sulfur bond distances, which may be expected to apply to other structurally unconstrained complexes.

(b) $Na(Ph_4As)[Fe(S_2\text{-}o\text{-xyl})_2]$ Acetonitrile Solvate. This was the first crystalline salt of the Fe(II) dianion to be isolated. In addition to the high mosaicity of the crystals, an additional problem in providing a complete crystal structure determination has been the uncertainty in the exact composition of the solvate components of the compound. Of the reasonable possibilities analytical data agree best with a ·2MeCN solvate, but the formulations ·2MeCN·H_2O, ·2MeCN·EtOH, and, marginally, ·MeCN·H_2O cannot be eliminated. As already described one acetonitrile solvate molecule was located in the x-ray study, but another solvate species containing the atom

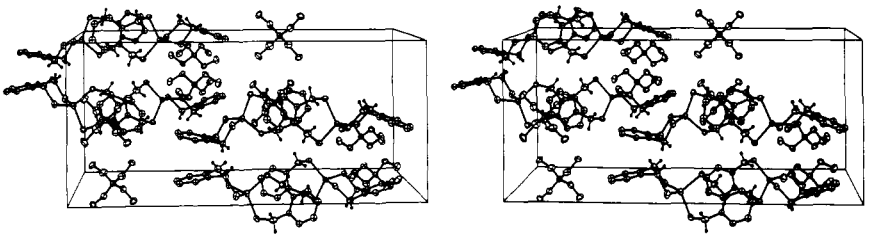

Figure 1. A stereoview of the unit cell of $(Et_4N)[Fe(S_2\text{-}o\text{-}xyl)_2]$. Atoms are drawn with 20% probability ellipsoids except for the hydrogen atoms, which are drawn artificially small. Hydrogen atoms on the cations and on the phenyl rings are omitted for the sake of clarity. The view is approximately down the x axis, with the y axis from left to right and the z axis from bottom to top.

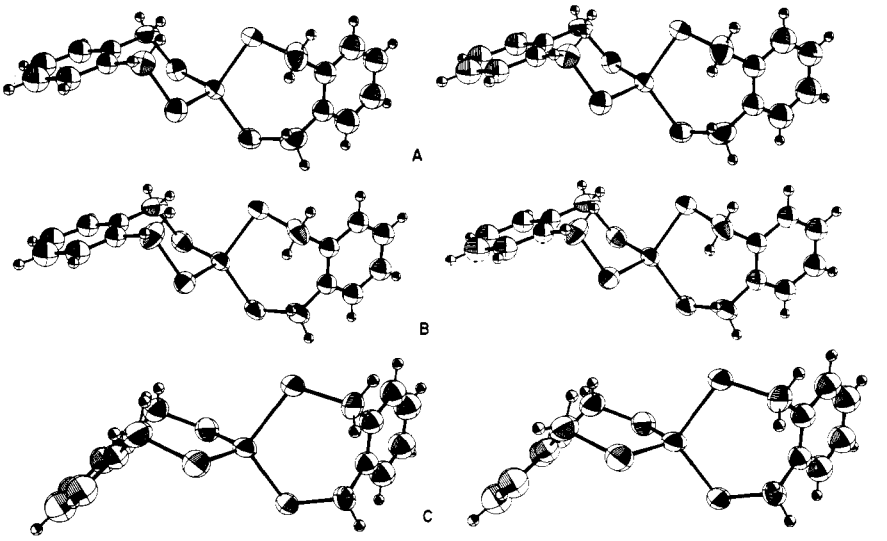

Figure 2. Stereoviews of the $[Fe(S_2\text{-}o\text{-}xyl)_2]^-$ (A,B) and $[Fe(S_2\text{-}o\text{-}xyl)_2]^{2-}$ (C) anions. In each view the 50% probability ellipsoids are displayed except for the hydrogen atoms, which are drawn artificially small.

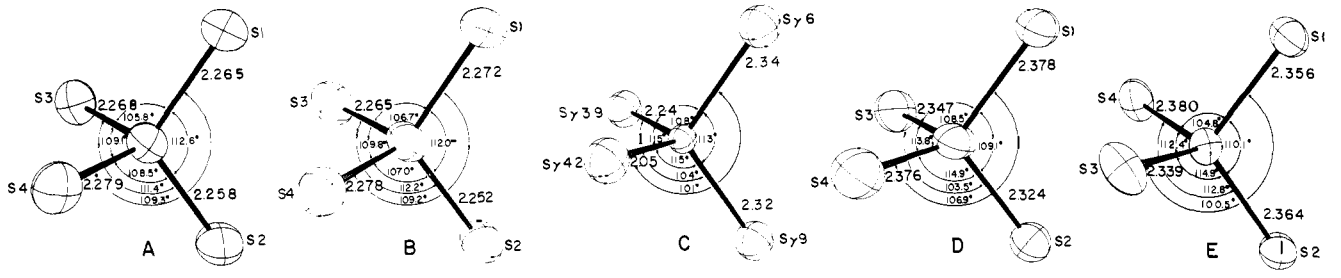

Figure 3. Geometries of the $Fe\text{-}S_4$ units in $[Fe(S_2\text{-}o\text{-}xyl)_2]^-$ (A,B), Rd_{ox} (C), $[Fe(S_2\text{-}o\text{-}xyl)_2]^{2-}$ (D), and $Fe[(SPMe_2)_2N]_2$ (E). The 50% probability ellipsoids are shown except for (C), where the scale is arbitrary. Note that the spatial orientation of these units is the same as in Figure 2, such that S1-S2 and S3-S4 define the chelate rings in A, B, and D. This arrangement applies to E as well, which was drawn using published data.[24]

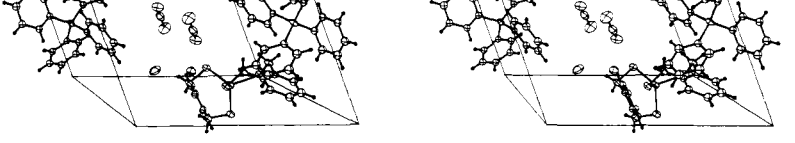

Figure 4. A stereoview of the unit cell of $Na(Ph_4As)[Fe(S_2\text{-}o\text{-}xyl)_2]$ acetonitrile solvate. The 20% thermal ellipsoids are shown except for the hydrogen atoms. The positions of the axes are the same as in Figure 1.

X could not be identified.[37b] Although other crystalline salts with simpler compositions were subsequently isolated, the structure of this compound was pursued. The resulting structural parameters (Table X), while not as precisely determined as might be desired, are of more than sufficient precision to allow a meaningful comparison between Fe(II,III)-S_4 coordination units.

A unit cell stereoview is given in Figure 4 and shows the structure to consist of well-separated cations and anions. As can be seen from this figure and the data of Table XII, atom X and the nitrogen atom of the ordered acetonitrile molecule are within van der Waals contact with the sodium ion; neither is within coordinating distance of Fe(II). Approximately octahedral coordination is completed about the sodium ion by

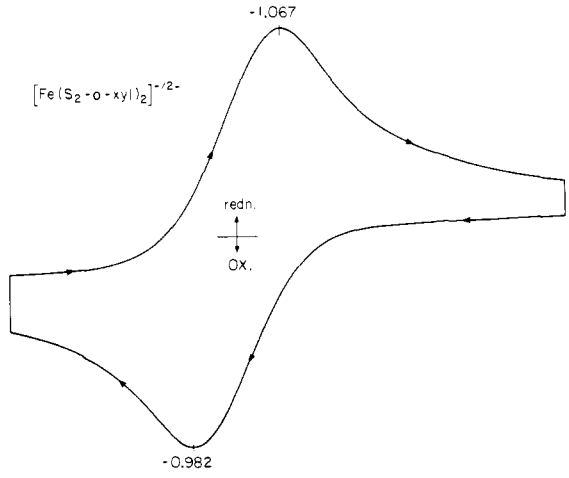

Figure 5. Cyclic voltammogram for the $[Fe(S_2\text{-}o\text{-}xyl)_2]^{-/2-}$ couple in DMF solution at a Pt electrode and a scan rate of 50 mV/s. Potentials are referenced to a SCE.

van der Waals contacts with two S(1) atoms, an S(3) atom, and an S(4) atom. The Ph_4As^+ cation shows no unusual trends in geometry (Table XII). The average As–C distance is 1.887 (15) Å, the standard deviation estimated from a population of four being roughly comparable with those of 0.008–0.012 Å estimated from the inverse matrix. The average C–As–C angle is 109.5 (2.3)°; there are clearly significant angular variations from tetrahedral symmetry, presumably arising as a result of packing forces.

As can be readily appreciated from Figure 2C and 3D, $[Fe(S_2\text{-}o\text{-}xyl)_2]^{2-}$ possesses overall an approximate tetrahedral structure, as does Rd_{red} based on the results of various physical measurements[11a] (vide infra) and preliminary x-ray observations at 4-Å resolution, which have indicated that upon dithionite reduction of a *C. pasteurianum* Rd_{ox} crystal the configuration of sulfur atoms around the iron atom had not changed.[19b] In the Fe(II)–S_4 coordination unit of the dianion Fe–S distances range from 2.324 (5) to 2.378 (5) Å with a mean value of 2.356 (13) Å, 0.089 (13) Å longer than the mean value for the two Fe(III) monoanions. The range and mean values of S–Fe–S angles are 103.5 (2)–114.9 (2)° and 109.5 (1.7)°, respectively. Average bite distances and angles are 3.89 Å and 111.5°, respectively, and the dihedral angle between FeS_2 planes is 94.3°. Thus the Fe(II)–S_4 coordination unit, as the Fe(III)–S_4 unit, approaches T_d symmetry, but rhombic distortions are clearly evident. While $[Fe(S_2\text{-}o\text{-}xyl)_2]^{2-}$ is also dissymmetric in the crystal (Figure 2C), chelate ring conformations are appreciably different from those exhibited by $[Fe(S_2\text{-}o\text{-}xyl)_2]^-$. The most significant change is in the internal Fe–S–C angles, which average 108.2° in the Fe(II) dianion and 101.5° in the two Fe(III) monoanions. This change is reflected in another way by the dihedral angles between the FeS_2 and C_2S_2 planes (Table X). In essence the iron atom lies closer to the C_2S_2 plane in the Fe(II) than in the Fe(III) complex. As a result of the longer Fe–S distances in $[Fe(S_2\text{-}o\text{-}xyl)_2]^{2-}$ the S···S bite distance is greater and this, together with the tendency of the sulfur atoms toward a tetrahedral distribution of bonding and lone-pair electrons, brings about this conformational change.

In both structures we have been unable to identify clearly cation–anion or solvate–anion interactions or chelate ring conformations as sources of degradation of Fe(II,III)–S_4 coordination units from idealized T_d microsymmetry. As has been noted, the structures of the two independent Fe(III) monoanions are virtually identical. Further, the Fe(II)–S_4 units in $[Fe(S_2\text{-}o\text{-}xyl)_2]^{2-}$ (Figure 3D) and $Fe[(SPMe_2)_2N]_2$[24] (Figure 3E) are in reasonable agreement, with average Fe–S distance and S–Fe–S angle values in the latter being 2.360 (9) Å and 109.3 (2.2)°, respectively. Thus, it appears that the coordination unit in $[Fe(S_2\text{-}o\text{-}xyl)_2]^{2-}$ is probably not significantly distorted as a result of the packing of ionic units in the unit cell, including the van der Waals interaction of the sodium atom with particular sulfur atoms. One possible source of distortions in the Fe(II) complexes (^5E T_d ground state) is the Jahn–Teller effect; Jahn–Teller distortions are absent in the tetrahedral Fe(III) case ($^6A_1$ ground state). We conclude that the coordination geometries of $[Fe(S_2\text{-}o\text{-}xyl)_2]^-$ and $[Fe(S_2\text{-}o\text{-}xyl)_2]^{2-}$, on which no symmetry is crystallographically imposed, are near representations of the configurations which would arise in the absence of perturbative crystalline and ligand structural effects; i.e., they closely approach the limit of unconstrained Fe(II,III)$(SR)_4$ stereochemistries. Further discussion of structural properties is deferred to a later section.

Electron Transfer Properties. The conversion of $[Fe(S_2\text{-}o\text{-}xyl)_2]^{2-}$ to $[Fe(S_2\text{-}o\text{-}xyl)_2]^-$ upon reaction with dioxygen suggests that these two species should be interconvertible by a simple one-electron transfer reaction, a property obligatory to their designation as Rd analogues. Previously it had been shown that in DMF $[Fe(S_2\text{-}o\text{-}xyl)_2]^-$ reduces at a Pt electrode with $E_{1/2} = -1.03$ V and a slope of −67 mV (−57 mV at a DME) evaluated from a plot of $\log[i/(i_d - i)]$ vs. E.[26] Cyclic voltammetric parameters suggested a kinetically quasi-reversible[38] process. A voltammogram recorded at 50 mV/s is shown in Figure 5. The constant peak current ratio $i_{p,c}/i_{p,a} = 1.03 \pm 0.03$ at scan rates of 10–500 mV/s indicates stability of the reduced form which was considered, but not proven, to be $[Fe(S_2\text{-}o\text{-}xyl)_2]^{2-}$. Anodic polarography of the Fe(II) complex in DMF (Pt electrode) reveals a one-electron oxidation at −1.02 V (slope 63 mV) and no other oxidation waves to −0.3 V, thereby confirming the existence of the couple $[Fe(S_2\text{-}o\text{-}xyl)_2]^- + e^- \rightleftharpoons [Fe(S_2\text{-}o\text{-}xyl)_2]^{2-}$. When simply converted to the standard hydrogen electrode reference without further correction this couple is ca. 0.7 V more negative than potentials for the Rd_{ox}/Rd_{red} couple.[12a,14a] Substantially more negative potentials in nonaqueous media compared to protein potentials in aqueous solution are features common to all 1-, 2-, and 4-Fe synthetic analogues.[4,10,39] For the latter analogues differences are reduced to ca. 100–150 mV more negative than Fd_{ox}/Fd_{red} protein values when potentials of both analogues and proteins are measured polarographically in the same media.[40] Similar experiments have not as yet been conducted for Rd proteins and the 1-Fe analogues described here. When examined in DMF solution (Pt electrode) $[Fe_2(s_2\text{-}o\text{-}xyl)_3]^{2-}$ shows two oxidation waves. These occur at $E_{1/2} = -0.63$ and −0.07 V with slopes of 98 and 148 mV, respectively, and a diffusion current ratio of 1:1. In view of the irreversible nature of these two processes, no chemical attempts to prepare oxidation products of the binuclear dianion have been made.

Mössbauer Spectra. (a) $[Fe(S_2\text{-}o\text{-}xyl)_2]^-$. The zero-field and magnetically perturbed Mössbauer spectra of the high-spin Fe(III) analogue have been presented previously,[26] and relevant data are collected in Table XIII. The most important results are the following: (i) low temperature zero-field spectra consist of a single quadrupole doublet and are consistent with a high-spin Fe(III)–S_4 unit distorted from T_d symmetry; (ii) the existence of a quadrupole splitting (ΔE_Q) in frozen solution indicates that upon release from a crystalline environment a noncubic stereochemistry persists; (iii) the close agreement between internal hyperfine magnetic fields at the ^{57}Fe nucleus (H_{hf}), evaluated from spectra of $[Fe(S_2\text{-}o\text{-}xyl)_2]^-$ obtained in an applied magnetic field $H_0 = 80$ kOe, imply similar bond covalency effects in the analogue and Rd_{ox}.

(b) $[Fe(S_2\text{-}o\text{-}xyl)_2]^{2-}$. Mössbauer spectra were obtained for crystalline samples of $Na(Ph_4As)[Fe(S_2\text{-}o\text{-}xyl)_2]$, containing high-spin Fe(II), between 1.4 K and room temperature.

Table XIII. Magnetic and Mössbauer Data for Tetrahedral Fe(II,III)–S_4 Compounds

Compd	μ, μ_B	Mössbauer data				
		T, K	δ, mm/s[a]	ΔE_Q, mm/s	Sign of V_{zz}	H_{hf}, kOe
$(Et_4N)[Fe(S_2\text{-}o\text{-xyl})_2]$[b]	5.92	77	0.13[c]	0.57[c]		−380[g]
Rd_{ox}	5.85[e]	77	0.25[d,k]	0.74 (?)[e]		−370[f,g]
$Na(Ph_4As)[Fe(S_2\text{-}o\text{-xyl})_2]$	5.10[m]	295	0.61[h]	3.20[h]		
		77	0.61	3.28		
		4.2	0.61	3.34	(−)	−128[l]
		1.4	0.61	3.32		
$(Ph_4P)_2[Fe(SPh)_4]$[i]	5.02[j]	77	0.64	3.24	(−)	
Rd_{red}[f,k]	5.05[e]	77	0.65	3.16	(−)	−193[g,l]

[a] Relative to Fe metal. [b] Reference 26. [c] ±0.02. [d] Reference 18b. [e] Reference 13. [f] Reference 18a. [g] At 4.2 K. [h] Values of δ (±0.03) and ΔE_Q (±0.05) were obtained from computer fits to observed spectra and have the indicated uncertainties at all temperatures. [i] Reference 42. [j] Reference 23. [k] In comparing protein and analogue results it should be noted that no second-order Doppler shift correction has been applied to the results of ref 18a and b, where (in contrast to this work) measurements were taken with source and absorber at different temperatures. [l] At H_0 = 60 kOe. [m] Bis(tetraethylammonium) salt at 80 K.

Spectral parameters are listed in Table XIII and spectra at H_0 = 0 are shown in Figure 6. At each temperature the spectrum consists of a single symmetric quadrupole doublet. Values of isomer shifts (δ) and ΔE_Q are comparable with those measured in other iron compounds with distorted tetrahedral Fe–S_4 coordination units. Isomer shifts of the oxidized and reduced analogues are consistent with the values of 0.2 and 0.6 mm/s proposed by Reiff et al.[41] as diagnostic of high-spin Fe(III)–S_4 and Fe(II)–S_4, respectively. More recently, Kostikas et al.[42] have measured the Mössbauer parameters of several tetrahedral Fe(II)–S_4 complexes,[22,23] including $[Fe(SPh)_4]^{2-}$ (Table XIII). Their values at 77 K are entirely similar to those of $[Fe(S_2\text{-}o\text{-xyl})_2]^{2-}$, whose isomer shift and quadrupole splitting in turn closely match those of *C. pasteurianum* Rd_{red}.[18a]

In a ligand field of T_d symmetry the free ion ^5D term of Fe(II) is split into a lower $^5E(e^3t_2^3)$ and upper $^5T_2(e^2t_2^4)$ state separated by $\Delta_t \sim 5000$–6000 cm^{-1} (vide infra). In this exact symmetry no quadrupole splitting is expected because the two component states of the ground orbital doublet contribute equal and opposite values to the electric field gradient (EFG) at the nucleus. Distortions from T_d symmetry observed with $Na(Ph_4As)[Fe(S_2\text{-}o\text{-xyl})_2]$ result in a lifting of the ground-state orbital degeneracy and a finite quadrupole splitting. The structural parameters for the Rd_{red} site have not been determined. Because the Fe(II)–S_4 unit of $[Fe(S_2\text{-}o\text{-xyl})_2]^{2-}$ is too unsymmetrical to be classified in a rotational subgroup of T_d, and all quintet states derive from the same free ion term, it is somewhat more convenient to present a low-symmetry d^6 energy diagram in terms of individual d orbitals (Figure 7). As in a previous treatment of Rd_{red},[11a] orbital separations are approximated to spectroscopic energies inasmuch as all quintet states have the same mutual electron repulsion parameters. From the small temperature dependence of ΔE_Q observed over the temperature range 1.4–295 K (Table XIII), an estimate of the energy separation between the ground orbital to the next excited state can be obtained by fitting the experimental data to an equation of the form $\Delta E_Q(T) = \Delta E_Q(0) \tanh(\Delta/2kT)$ expected for the thermal population of the two isolated orbital levels, d_{z^2} and $d_{x^2-y^2}$, split by an energy Δ. $\Delta E_Q(0)$ is the quadrupole splitting at zero temperature where only the ground orbital state is populated and $\Delta E_Q(T)$ is its value at temperature T. Here we have assumed that Δ is much larger than any splittings due to the spin–orbit interaction and the direct lattice contribution to the EFG has been neglected. By using $\Delta E_Q(0)$ = 3.32 mm/s, the value observed at 1.4 K, the lowest temperature of measurement, an estimate of $\Delta \simeq 900$ cm^{-1} is obtained. The temperature dependence observed by Rao et al.[18a] for Rd_{red} is somewhat smaller than that of $Na(Ph_4As)$-$[Fe(S_2\text{-}o\text{-xyl})_2]$. The latter, however, is very similar to that of freeze-dried (powder) Rd_{red} observed by Phillips et al.[13] for which Eaton and Lovenberg[11a] estimate $\Delta \simeq 850$ cm^{-1}. Owing to the experimental error associated with the values of ΔE_Q and the small temperature dependence, these values of Δ are probably accurate within ±100 cm^{-1}.

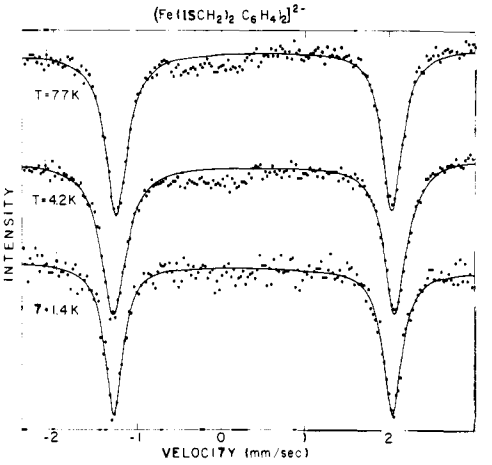

Figure 6. Mössbauer spectra of $Na(Ph_4As)[Fe(S_2\text{-}o\text{-xyl})_2]$ at various temperatures. The solid lines give least-squares fits of the experimental points to Lorentzian lines. The small broad feature centered above 0 mm/s is presumably due to an Fe(III) impurity.

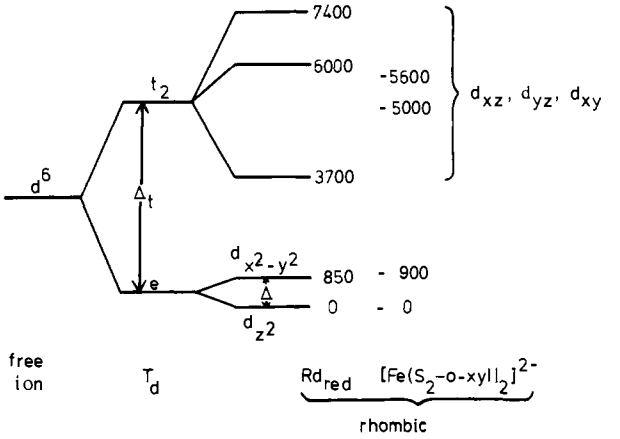

Figure 7. d-Orbital energy level diagram for Fe(II) in T_d and distorted tetrahedral ligand fields. Orbital energies for Rd_{red} are taken from ref 11a.

To characterize further the ground state of the Fe(II) ion, Mössbauer spectra in externally applied magnetic fields, in longitudinal geometry, were obtained. As discussed by Collins[43] and Gabriel and Ruby,[44] when the line width is taken into account, the superposition of the absorption lines arising from transitions between the magnetically perturbed nuclear levels in the presence of the randomly oriented EFG tensor in a powder absorber results in the splitting of the $|\frac{1}{2}, \pm\frac{1}{2}\rangle \rightarrow |\frac{3}{2},$

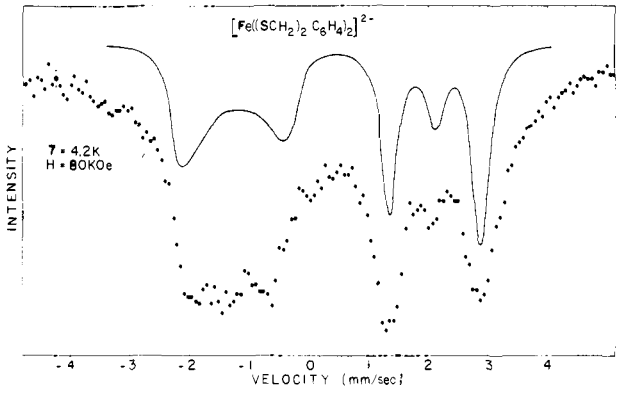

Figure 8. Mössbauer spectrum of $Na(Ph_4As)[Fe(S_2\text{-}o\text{-}xyl)_2]$ at 4.2 K in an external field of 80 kOe applied parallel to the γ-ray direction. The solid line is theoretical for a powder sample with $\Delta E_Q = 3.32$ mm/s and an effective magnetic field of 63 kOe with longitudinal configuration. The differences between the experimental data and calculated curve are due to anisotropy of the hyperfine interaction in the sample.

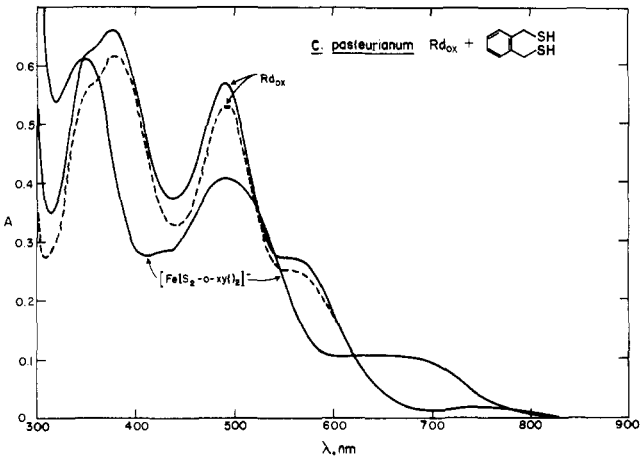

Figure 9. Absorption spectra: - - -, Rd_{ox} in aqueous solution (50 mM TrisCl, pH 8.5); —, (60 μM Rd_{ox} in 4:1 v/v Me_2SO/H_2O); — (lower curve), $[Fe(S_2\text{-}o\text{-}xyl)_2]^-$ in 4:1 v/v Me_2SO/H_2O formed by adding 40 μl of 0.24 M o-xyl$(SH)_2$ to 1 ml of the preceding solution. This spectrum was recorded 1 h after dithiol addition.

$\pm 3/2\rangle$ transition line into an apparent doublet and the $|1/2, \pm 1/2\rangle \rightarrow |3/2, \pm 1/2\rangle$ line into an apparent triplet. The spectrum of $Na(Ph_4As)[Fe(S_2\text{-}o\text{-}xyl)_2]$ in the presence of a magnetic field of 80 kG at 4.2 K is shown in Figure 8. The lower velocity absorption line of the quadrupole doublet observed in the absence of an external magnetic field has been split into a doublet and the higher velocity absorption line into a triplet, indicating that the sign of the principal component of the EFG, V_{zz}, is negative. Similar spectra were obtained at lower values of the applied field as well as at higher absorber temperatures. The negative sign of V_{zz} demonstrates that the ground-state orbital of the Fe(II) ion has d_{z^2} symmetry, as has previously been shown for Rd_{red}.[18a] Comparisons of the observed spectra with computer-generated spectra reveal that the observed field at the nucleus H_n differs from the applied magnetic field, H_0, indicating the presence of a magnetic hyperfine interaction induced by the applied field. For $H_0 = 60$ kOe, $|H_n| = 68.5$ kOe; for $H_0 = 80$ kOe, $|H_n| = 63$ kOe. Since H_n decreases as H_0 increases from 60 to 80 kOe, we infer that the sign of the magnetic hyperfine interaction expressed as an effective magnetic field, H_{hf}, is negative. Writing $\vec{H}_n = \vec{H}_0 + \vec{H}_{hf}$, the 60 and 80 kOe spectral parameters yield $H_{hf} = -128$ and -143 kOe, respectively. The parameters obtained at 1.4 K yield the same value of H_{hf} as those obtained at 4.2 K for $H_0 = 60$ and 80 kOe. The fact that $|H_{hf}|$ continues to increase as H_0 increases from 60 to 80 kOe implies a zero-field splitting of the electronic ground state of the order of several degrees. The full saturation value of the magnetic hyperfine interaction constant would not be observed until μH_0 is large compared with the zero-field splitting.

The magnetic hyperfine interactions induced by the applied field in the present case compare with those observed by Rao et al.[18a] in Rd_{red} as follows. For $H_0 = 60$ kOe, they obtained $H_{hf} = -193$ kOe at temperatures between 4.2 and 1.3 K. However, as discussed above, if there is a zero-field splitting, this does not represent the full saturation value. If we assume comparable zero-field splittings in the two cases, then the difference in the hyperfine interaction reflects a difference in the orbital character of the ground state. According to Marshall and Johnson[45] the magnetic hyperfine interaction arises from three principal contributions,

$$H_{hf} = H_C + H_L + H_D \qquad (2)$$

where H_C is the core polarization contribution arising from the Fermi contact interaction, H_L is the orbital moment contribution, and H_D is the field produced by the dipolar interaction with the spin moment of the iron atom. H_D is proportional to the EFG at the nucleus and is thus virtually the same in the two cases. It is also reasonable to assume H_C to be comparable. This leaves H_L to account for the difference, with a slightly larger orbital contribution in the present case. This implies a larger value of Δ in Rd_{red}, which is consistent with the smaller temperature variation of ΔE_Q in Rd_{red}, but the experimentally determined Δ values for the protein and $[Fe(S_2\text{-}o\text{-}xyl)_2]^{2-}$ are insufficiently accurate to establish this point.[46]

In summary, the Mössbauer parameters δ, ΔE_Q, H_{hf} collected in Table XIII, together with the approximate values of the ground orbital doublet splitting Δ, convincingly demonstrate that $[Fe(S_2\text{-}o\text{-}xyl)_2]^{2-}$ and *C. pasteurianum* Rd_{red} have similar Fe(II)-S_4 geometries, ground-state electronic structures, and Fe-S bond covalency properties. This similarity doubtless extends to other Rd_{red} proteins such as, e.g., that from *Ch. ethylica*.[18a] In this context the available data indicate that $[Fe(SPh)_4]^{2-}$ [23,42] is also an entirely suitable ground-state analogue of Rd_{red}.

Electronic Absorption Spectra. (a) $[Fe(S_2\text{-}o\text{-}xyl)_2]^-$. The spectrum of this complex in DMF solution has been reported earlier[26] and resembles that of Rd_{ox} proteins in aqueous solution. Rd_{ox} chromophores are characterized by an intense two-band system at ~380 and ~490 nm, a less intense feature at ~560 nm, and a much weaker band at ~745 nm. The spectrum of *C. pasteurianum* Rd_{ox} (Table XIV) is typical and at least the three higher energy bands, as previously discussed,[11a,47] arise from S → Fe charge-transfer excitations. To provide a more direct comparison between protein and analogue spectra a solution of *C. pasteurianum* Rd_{ox} in 4:1 v/v Me_2SO/H_2O was treated with sufficient o-xyl$(SH)_2$ to afford a dithiol/Fe mol ratio of 160:1 (Figure 9). The system exhibited slow spectral changes with the final spectrum, obtained after 1 h, being identical with that of $[Fe(S_2\text{-}o\text{-}xyl)_2]^-$ measured separately. Consequently, the spectral changes arise from the reaction

$$Rd_{ox} + 2\ o\text{-xyl}(SH)_2 \rightarrow [Fe(S_2\text{-}o\text{-xyl})_2]^- + \text{apo-Rd} \qquad (3)$$

similar in kind to reactions which extrude Fe_2S_2 and Fe_4S_4 active site cores of Fd proteins under the same or similar experimental conditions.[48] Using the extinction coefficient data in Table XIV it was found that 1.1 g-atom of Fe/mol protein was removed. The analogue spectrum is dominated by two intense bands at 354 and 487 nm which doubtless correspond to the somewhat more intense protein features at 376 and 490 nm in Me_2SO/H_2O water solution. More pronounced differences are evident in the 550-800-nm range, with the broad

Table XIV. Solution Absorption Spectral Data for *o*-Xylyldithiolato Metal(II,III) Complexes, Rd_{ox}, and Rd_{red}

Compd	Solvent	λ_{max}, nm (ϵ^a)
$(Et_4N)[Fe(S_2\text{-}o\text{-xyl})_2]$	DMF	688 (1670), ~640 (1600), 486 (6240), ~450 (sh, 4300), 354 (8300)
	Me_2SO/H_2O^b	~660 (1480), 487 (5400), ~425 (3800), 354 (7850)
Rd_{ox}^c	Me_2SO/H_2O^b	745, 560 (sh), 490, 376
	H_2O^d, crystal[h]	746 (360), 565 (~4000), 490 (8850), 380 (10 800)
$(Et_4N)_2[Fe(S_2\text{-}o\text{-xyl})_2]$	MeCN	~2000 (109, sh),[f] 1800 (123), $[^5E \rightarrow {}^5T_2]$
	DMF	~450 (sh, 390), ~355 (sh, 2660), 323 (7710)
	Me_2SO/H_2O^b	~352 (sh, 3290), 320 (6320)
$Na(Ph_4As)[Fe(S_2\text{-}o\text{-xyl})_2]$	DMF	~450 (sh, 410), ~355 (3070), 322 (7410)
Rd_{red}^c	D_2O[g]	~2700, 1600 (130) $[^5E \rightarrow {}^5T_2]$
	H_2O^d	333 (6300), 311 (10 800)
	$Me_2SO/H_2O^{b,e}$	338, 315
$(Et_4N)_2[Fe_2(S_2\text{-}o\text{-xyl})_3]$	Me_2SO	1930 (175) $[^5E \rightarrow {}^5T_2]$
	DMF	360 (8570)
$(Et_4N)_2[Co(S_2\text{-}o\text{-xyl})_2]$	MeCN	1550 (242), ~1380 (sh, 190) $[^4A_2 \rightarrow {}^4T_1(F)]$
	DMF	788 (460), 684 (645), 610 (481) $[^4A_2 \rightarrow {}^4T_1(P)]$, 355 (3450)
$(Et_4N)_2[Ni_2(S_2\text{-}o\text{-xyl})_3]$	DMF	~620 (sh, 524), 486 (3760)

[a] M^{-1} cm^{-1}. [b] 4:1 v/v, aqueous portion 50 mM in TrisCl, pH 8.5. [c] *C. pasteurianum*. [d] Reference 14a. [e] Principal bands. [f] Poorly defined feature. [g] Reference 15. [h] Reference 11a.

Table XV. Ligand Field Spectral Parameters[a] for Tetrahedral Co(II)–S_4 and Fe(II)–S_4 Complexes

Complex	ν_2	ν_3	Δ_t	B'	Ref[b]
$Co[(SPPh_2)_2CH]_2$	6540	14 970	3800	675	20b
$Co[(SPMe_2)_2N]_2$	6580	14 400	3840	631	20a
$[Co(SPh)_4]^{2-}$	6900	14 800[d]	4030	643	23
$[Co(S_2\text{-}o\text{-xyl})_2]^{2-}$	6980[c]	14 570[c]	4090	619	*e*
	7250	14 620[d]	4270	604	*e*
$[Co(12\text{-peptide})]^{2-}$	7330	15 100	4300	636	21
$[Co(dts)(SPh)_2]^{2-}$	8200	15 490[d]	4880	603	23
$[Co(dts)_2]^{2-}$	8300	15 100	4980	564	22

	$\Delta_t \sim \nu[^5E \rightarrow {}^5T_2]$	Ref
$Fe[(SPMe_2)_2N]_2$	~3500 (split)	20a
$[Fe(12\text{-peptide})]^{2-}$	~5100 (broad)	21
$[Fe(S_2\text{-}o\text{-xyl})_2]^{2-}$	5560	*e*
$[Fe(dts)_2]^{2-}$	5800	22
$[Fe(SPh)_4]^{2-}$	5880	23
Rd_{red}	6250 (~5000)	11a, 15

[a] cm^{-1}. [b] Source of transition energy data. [c] Data calculated using intensity-weighted ν_2,max and average of ν_3 bands. [d] Data calculated using central ν_3 band. [e] This work.

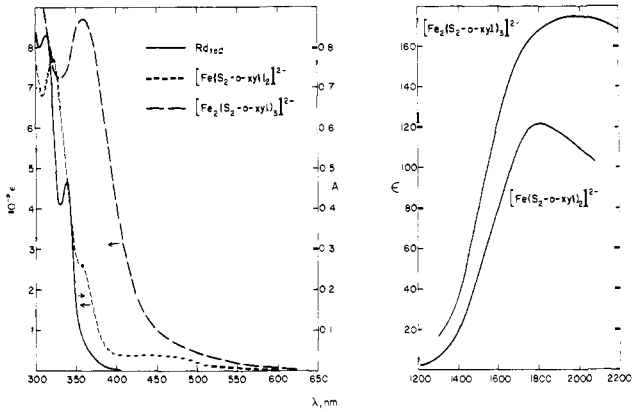

Figure 10. Absorption spectra: left, Rd_{red} and $[Fe(S_2\text{-}o\text{-xyl})_2]^{2-}$ in 4:1 v/v Me_2SO/H_2O with aqueous component containing 50 mM TrisCl (pH 8.5), $[Fe_2(S_2\text{-}o\text{-xyl})_3]^{2-}$ in DMF; right, near-infrared spectra of $[Fe(S_2\text{-}o\text{-xyl})_2]^{2-}$ in acetonitrile and $[Fe_2(S_2\text{-}o\text{-xyl})_3]^{2-}$ in Me_2SO.

analogue absorption near 660 nm perhaps being the red-shifted counterpart of the protein absorption at 560 nm. Specific band assignments are not warranted at this time, but may be possible upon completion of SCF-Xα-SW calculations of model $Fe(SR)_4^-$ chromophores, for which preliminary results have recently been published.[49] On an empirical basis the comparative spectra in Figure 9 indicate a similarity, but certainly not an identity, between analogue and protein chromophores, a matter qualitatively consistent with the foregoing structural and Mössbauer spectral results.

(b) $[Fe(S_2\text{-}o\text{-xyl})_2]^{2-}$. In contrast to the ready occurrence of reaction 3, Rd_{red} did not react with excess *o*-xyl$(SH)_2$ within 1 h under the same conditions. The spectra in Figure 10 were obtained on separately measured samples. Spectra in the UV region of both the analogue and Rd_{red} are dominated by two intense charge-transfer bands, shifted as expected to higher energies compared with the Fe(III) case.[50] In Me_2SO/H_2O the bands of $[Fe(S_2\text{-}o\text{-xyl})_2]^{2-}$ (320, 352 nm) exhibit small red shifts compared with those of *C. pasteurianum* Rd_{red} (315, 338 nm), but a close degree of spectral similarity is evident. A somewhat more direct probe of electronic properties is provided by ligand-field spectra, which for Fe(II) in T_d symmetry consist of the single transition $^5E \rightarrow {}^5T_2$ found in the near-infrared region for simple inorganic complexes.[51] From a combination of absorption and CD measurements Eaton and Lovenberg[11a] have deduced the orbital splittings in Figure 7 for *C. pasteurianum* Rd_{red}. Measurements of $[Fe(S_2\text{-}o\text{-xyl})_2]^{2-}$ were confined to solution absorption spectra (Table XIV, Figure 10), which reveal a well-defined maximum at 1800 nm (5560 cm^{-1}) and an indication of an unresolved band near 2000 nm (5000 cm^{-1}). These results indicate a small splitting of the t_2 orbitals, consistent with the lack of symmetry of the complex. In such cases the single parameter Δ_t is inadequate to describe orbital splittings, but in the absence of fully resolved spectra it has been approximated to the principal band energy as an empirical modulus of ligand-field strength. Results for $[Fe(S_2\text{-}o\text{-xyl})_2]^{2-}$ and related complexes are collected in Table XV, from which it is seen that thiolate sulfur induces an effective Δ_t of ca. 5000–6000 cm^{-1}. A corresponding value of Δ_t for Rd_{red} is uncertain owing to the large t_2 orbital splitting, but the same approximation or the mean of the orbital energies leads to 6250 or 5700 cm^{-1}, respectively. Δ_t has otherwise been approximated as ~5000 cm^{-1}.[11a] Consequently, it follows that the average ligand-field strength in Rd_{red} and $[Fe(S_2\text{-}o\text{-xyl})_2]^{2-}$ are comparable (vide infra), but the t_2 orbital total splitting in the protein may be larger, reflecting a more distorted metal site geometry.

(c) $[Fe_2(S_2\text{-}o\text{-xyl})_3]^{2-}$. This highly oxygen-sensitive complex, an unexpected product during initial attempts[26] to synthesize a Rd_{red} analogue, has not been studied in detail and as yet single crystals suitable for x-ray studies have not been obtained. Its absorption spectrum (Figure 10) clearly distinguishes it from $[Fe(S_2\text{-}o\text{-xyl})_2]^{2-}$ in the UV region and identifies the Fe(II) coordination site as essentially tetrahedral on the basis of the broad band at 5200 cm^{-1} (ϵ_{Fe} 88). Low-temperature

Mössbauer spectra reveal a diamagnetic ground state, which must arise from antiparallel spin coupling. If $[Fe_2(S_2\text{-}o\text{-}xyl)_3]^{2-}$ is dimeric, likely structures are **1** and **2**. One of these

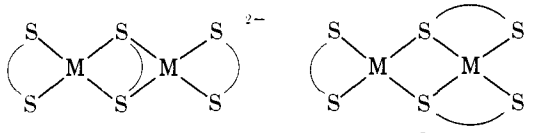

1 2

structures may also apply to $[Fe_2(SCH_2(S)CH_2CH_2OH)_3]^{2-}$, identified in solution,[52] if it is actually binuclear; this is the only Fe(II) thiolate complex previously reported with the same stoichiometry as $[Fe_2(S_2\text{-}o\text{-}xyl)_3]^{2-}$. The μ_2-thiolato mode of bridging has been established by x-ray studies of several dimeric Fe(II) complexes.[53]

(d) $[Co(S_2\text{-}o\text{-}xyl)_2]^{2-}$. This compound, prepared as its Fe(II) analogue using ca. 3.5:1 dithiol/Co mol ratio, was sought in order to utilize the spectroscopically informative tetrahedral Co(II) chromophore[51,54] in a further examination of the ligand-field properties of $S_2\text{-}o\text{-}xyl^{2-}$ and other sulfur-containing ligands. The magnetic moment (4.48 (20 K)–4.60 μ_B (280 K)) and absorption spectrum (Table XIV, Figure 11) of $[Co(S_2\text{-}o\text{-}xyl)_2]^{2-}$ demonstrate that this complex possesses the desired stereochemistry. In T_d symmetry Co(II) has three spin-allowed ligand-field transitions, of which $^4A_2 \rightarrow {}^4T_1(F)$ (ν_2) and $^4A_2 \rightarrow {}^4T_1(P)$ (ν_3) occur in the visible and near-infrared regions.[51] The spectrum of $[Co(S_2\text{-}o\text{-}xyl)_2]^{2-}$ reveals a split ν_2 band and an especially clear case of resolution of ν_3 into three components whose separations (1930, 1770 cm^{-1}) are unlikely to arise from spin–orbit coupling effects only. Thus this complex, as $[Fe(S_2\text{-}o\text{-}xyl)_2]^{2-}$, possesses a tetrahedral chromophore with rhombic distortion. Following the usual practice in such cases, T_d microsymmetry was assumed, spin–orbit interactions were neglected, and the parameters Δ_1 and B' were evaluated from the equations

$$\Delta_1^2 - 0.529(\nu_2 + \nu_3)\Delta_1 + 0.294\nu_2\nu_3 = 0 \quad (4)$$

$$B' = (\nu_2 + \nu_3 + 3\Delta_1)/15 \quad (5)$$

derived by standard procedures of ligand-field theory. Results for $[Co(S_2\text{-}o\text{-}xyl)_2]^{2-}$ and other Co(II)–S_4 chromophores (in all cases recalculated from available literature data) are collected in Table XV, from which several points emerge. (i) For sulfur-containing ligands the spectrochemical series (6) is obtained, in which the equal rank of $S_2\text{-}o\text{-}xyl^{2-}$ and 12-peptide^{4-} further emphasizes the electronic similarity between simple alkylthiolate and cysteinate ligands. (ii) Based on previous compilations of Δ_1 and B′ data,[51,54] thiolate ligands rank between chloride or azide and nitrogen-bonded thiocyanate in the more general series (7)[55] and are devoid of unusual nephelauxetic effects as manifested in values of B'. Consequently, it may be inferred that cysteinate groups, as all other coordinating peptide side chains in metalloproteins,

$$(SPR_2)_2N^- \sim (SPR_2)_2CH^- < SPh^- \lesssim S_2\text{-}o\text{-}xyl^{2-} \lesssim 12\text{-peptide}^{4-} < dts^{2-} \quad (6)$$

$$I^- < Br^- < Cl^- < N_3^- < SPh^- \lesssim S_2\text{-}o\text{-}xyl^{2-} \lesssim 12\text{-peptide} \sim OH^- \sim NCO^- < NCS^- \quad (7)$$

are intrinsically weak-field ligands.[56] In their analysis of the Rd_{red} spectrum Eaton and Lovenberg,[11a] prior to the availability of the data in Table XV, considered their estimate of $\Delta_1 \sim 5000$ cm^{-1} as disquieting, presumably because it exceeded values for halide complexes[51] and Fe(II) in sulfide lattices,[57] and suggested that protein conformational constraints could be responsible. The current data support the view that the average ligand field strength in Rd_{red} is consistent with the expectations from the series in (6), i.e., in this sense the protein chromophore is unexceptional.

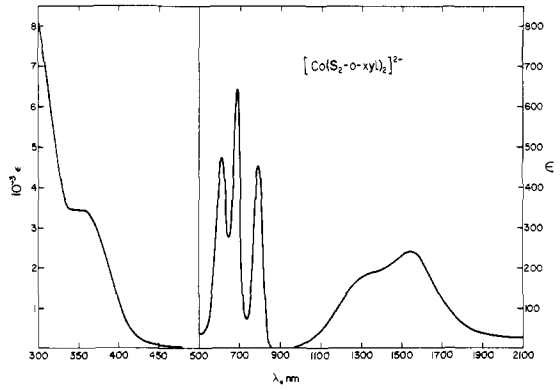

Figure 11. Absorption spectrum of $[Co(S_2\text{-}o\text{-}xyl)_2]^{2-}$ in acetonitrile (1000–2100 nm) and DMF (300–900 nm).

Although unrelated to the foregoing considerations, one additional aspect of the electronic spectrum of $[Co(S_2\text{-}o\text{-}xyl)_2]^{2-}$ is worthy of mention. This is the only well-defined synthetic Co(II)–thiolate complex for which spectral data in both the ligand-field and charge-transfer regions are available. The band at 355 nm (ϵ 3450, Figure 11) is very likely a S → Co(II) charge-transfer absorption and occurs at a wavelength close to that (340 nm, ϵ 15 500) found in the spectrum of horse liver alcohol dehydrogenase (LADH) in which all four Zn(II) atoms of the native enzyme have been replaced by Co(II).[58] In its native form this enzyme has two catalytic and two structural sites containing the coordination units $[Zn(S\text{-}Cys)_2(His)(H_2O)]$ and $[Zn(S\text{-}Cys)_4]$,[59] respectively. The nature of coordination in "blue" copper proteins is an unresolved matter at present. Substitution of Cu(II) by Co(II) in stellacyanin affords a chromophore which contains ligand-field features suggestive of distorted tetrahedral coordination and a higher energy band (355 nm, $\epsilon \sim 1200$) assigned as S → Co(II) charge transfer.[60] The spectral results for $Co(S_2\text{-}o\text{-}xyl)_2^{2-}$ and Co_4(LADH) substantiate this assignment, and in the three species extinction coefficients occur in the range of ca. 900–1300/Co–S–Cys bond. Provided ligation modes are unchanged upon substitution, these results together with other recent spectroscopic evidence support the existence of one Cu–S–Cys interaction in the blue chromophore.[61,62]

(e) $[Ni_2(S_2\text{-}o\text{-}xyl)_3]^{2-}$. Despite the employment of a 3.4:1 dithiol/Ni mol ratio in synthesis, the product formed was the binuclear dianion (based on stoichiometry) rather than $[Ni(S_2\text{-}o\text{-}xyl)_2]^{2-}$ or $[Ni_3(S_2\text{-}o\text{-}xyl)_4]^{2-}$.[63] Tetrahedral $[Ni(SPh)_4]^{2-}$ is reported to be formed in the presence of excess ligand.[23] Larger excesses of dithiol have not been used in this work. $[Ni_2(S_2\text{-}o\text{-}xyl)_3]^{2-}$ is diamagnetic in the solid, exhibits one ligand-field band in the visible (Table XIV), and has no spectral features from 500 to 2000 nm, indicative of a nonplanar structure in solution. Structures **1** and **2** with planar coordination are considered likely for $[Ni_2(S_2\text{-}o\text{-}xyl)_3]^{2-}$ if binuclear; binuclear thiolate-bridged Ni(II) complexes related to these enjoy established precedents.[64] Tetrahedral and planar coordination in the Fe(II) and Ni(II) dimers, respectively, follow the usual stereochemical trends of these metal ions,[65] but the tetrahedral structure of $Ni[(SPR_2)_2N]_2$,[20a,66] contrasted to the planar stereochemistry of $Ni[(SPR_2)_2CH]_2$,[20b] remains difficult to rationalize.

Summary

The results presented for $[Fe(S_2\text{-}o\text{-}xyl)_2]^{2-}$ and those given here and elsewhere[26] for $[Fe(S_2\text{-}o\text{-}xyl)_2]^-$ indicate that these species are close electronic representations of Rd_{red} and Rd_{ox}, respectively. The collective data further suggest that metal ion site symmetries in Rd proteins may be somewhat more distorted from T_d symmetry than in the analogue, although it is

difficult to translate available spectroscopic differences into actual structural differences. We cannot assert at present that the 1-Fe complexes are as close structural analogues to Rd sites as are $[Fe_4S_4(SR)_4]^{2-}$ species to Fd_{ox} and HP_{red} sites.[4] However, we conjecture that the true structural disparity between $[Fe(S_2\text{-}o\text{-}xyl)_2]^-$ and Rd_{ox} may not be as large as that suggested by a comparison of Figures 3A, B, and C, and have previously cautioned[26] that designation of the *C. pasteurianum* Rd_{ox} site as entatic in the sense of Vallee and Williams[67] must await final refinement of the crystal structure.[6,19] Recently the structures of *Peptococcus aerogenes* Rd_{ox}[68] and *C. pasteurianum* Rd_{ox}[69] have been examined in lyophilized and frozen solution states by x-ray absorption spectroscopy. Preliminary analyses of the extended x-ray absorption fine structure (EXAFS) spectra suggest that Fe–S distances are probably closer to being equal than are the latest quoted values (Figure 3C) obtained by x-ray diffraction.

Redox events at a Rd site reduce to the elementary ligand-field description of the equation

$$Fe(III)(e^2t_2^3, S = 5/2) \underset{-e^-}{\overset{+e^-}{\rightleftharpoons}} Fe(II)(e^3t_2^3, S = 2) \qquad (8)$$

One state (Fe(III)) has no d-electron stereochemical influence and interconversion between the two states in a biological outer-sphere reaction proceeds by a change in population of the approximately nonbonding e orbitals (T_d symmetry) without any necessary intervention of rearranged (excited) d-electron configurations. One of the recognized contributions to the enthalpic barrier to electron transfer[70,71] is that of structural reorganization at the redox site in order to achieve the compromise geometry between Fe(II,III) ground-state minima, which serves as the transition state for electron gain or loss. If the Rd site is entatic, as previously proposed,[72] this component of the total enthalpic activation energy will be quite small. If on the other hand, the geometries of Rd_{ox} and Rd_{red} sites approach the unconstrained situations considered to be represented by $[Fe(S_2\text{-}o\text{-}xyl)_2]^-$ and $[Fe(S_2\text{-}o\text{-}xyl)_2]^{2-}$, respectively, the structures of the latter and related species provide a reasonable upper limit on the structural reorganization localized at the protein site. Defining δ = [Fe(II)–L]-[Fe(III)–L] and using mean distances, the following δ values are obtained for tetrahedral structural pairs: $[Fe(S_2\text{-}o\text{-}xyl)_2]^{2-}$, $Fe[(SPMe_2)_2N]_2/[Fe(S_2\text{-}o\text{-}xyl)_2]^-$, 0.09 Å; $[FeCl_4]^{2-}/[FeCl_4]^-$, 0.11 Å.[73,74] In the absence of protein constraints Fe–S distances in Rd upon oxidation would be expected to decrease by $\delta \sim 0.10$ Å, with about half this amount (together with associated angular changes) required to achieve the transition state. Values of stretching and bending force constants, currently unavailable, are required to estimate the structural reorganization energy in analogues and proteins. However, recent kinetic studies of *C. pasteurianum* Rd show that the protein undergoes very rapid outer-sphere redox and electron self-exchange reactions, and that activation barriers are dominated by entropic rather than enthalpic contributions.[75] When viewed against cases of slow outer-sphere rates where both structural and electronic configurational reorganization occur along the reaction coordinate,[76] it is evident, as noted by others as well,[70,75] that the architecture and oxidation levels of the Rd active site are such as to provide relatively lower structural and electronic reorganizational barriers to outer-sphere electron transfer. As discussed elsewhere,[4] this statement applies to other types of Fe–S protein sites. Indeed, it is difficult to imagine, given the weak-field nature of biological ligands and the requirement of an abundant metal, how the evolutionary construction of redox centers could have been more efficacious in minimizing these two types of barriers.

Acknowledgments. This research was supported at the Departments of Chemistry, M.I.T. and Stanford University, by National Institutes of Health Grants GM-19256, GM-22351, and GM-22352, at Northwestern University by National Institutes of Health Grant HL-13157, and at the Francis Bitter National Magnet Laboratory, M.I.T., by the National Science Foundation. We thank Professor L. E. Mortenson for a sample of rubredoxin and Professor Mortenson, Dr. C. L. Hill, and W. O. Gillum for experimental assistance. G.C.P. was partially supported by a National Institutes of Health Biomedical Sciences Support Grant administered by M.I.T.

Supplementary Material Available: tabular listings of idealized positions of hydrogen atoms (Table IV), root-mean-square amplitudes of vibration (Table V), values of F_o^2 and F_c^2 for $(Et_4N)[Fe(S_2\text{-}o\text{-}xyl)_2]$ (Table VI), and values of $10|F_o|$ and $10|F_c|$ for $Na(Ph_4As)[Fe(S_2\text{-}o\text{-}xyl)_2]$ acetonitrile solvate (Table IX) (70 pages). Ordering information is given on any current masthead page.

References and Notes

(1) Part 13. W. O. Gillum, R. B. Frankel, S. Foner, and R. H. Holm, *Inorg. Chem.*, **15**, 1095 (1976).
(2) (a) Stanford University; (b) Northwestern University; (c) Francis Bitter National Magnet Laboratory, M.I.T.
(3) R. H. Holm, *Endeavour*, **34**, 38 (1975).
(4) R. H. Holm and J. A. Ibers in "Iron–Sulfur Proteins", Vol. III, W. Lovenberg, Ed., Academic Press, New York, N.Y., in press, Chapter 7.
(5) W. H. Orme-Johnson, *Annu. Rev. Biochem.*, **42**, 159 (1973); G. Palmer in "The Enzymes", Vol. XII, Part B, 3d ed, P. D. Boyer, Ed., Academic Press, New York, N.Y., 1975, Chapter 1.
(6) L. H. Jensen, *Annu Rev. Biochem.*, **43**, 461 (1974).
(7) Protein abbreviations: Fd, ferredoxin; HP, "high-potential" iron protein; Rd, rubredoxin.
(8) (a) R. H. Holm, B. A. Averill, T. Herskovitz, R. B. Frankel, H. B. Gray, O. Siiman, and F. J. Grunthaner, *J. Am. Chem. Soc.*, **96**, 2644 (1974); (b) C. Y. Yang, K. H. Johnson, R. H. Holm, and J. G. Norman, Jr., *ibid.*, **97**, 6596 (1975); (c) R. W. Lane, A. G. Wedd, W. O. Gillum, E. Laskowski, R. H. Holm, R. B. Frankel, and G. C. Papaefthymiou, *J. Am. Chem. Soc.*, submitted for publication.
(9) (a) B. A. Averill, T. Herskovitz, R. H. Holm, and J. A. Ibers, *J. Am. Chem. Soc.*, **95**, 3523 (1973); (b) L. Que, Jr., M. A. Bobrik, J. A. Ibers, and R. H. Holm, *ibid.*, **96**, 4168 (1974).
(10) J. J. Mayerle, S. E. Denmark, B. V. DePamphilis, J. A. Ibers, and R. H. Holm, *J. Am. Chem. Soc.*, **97**, 1032 (1975).
(11) (a) W. A. Eaton and W. Lovenberg in "Iron–Sulfur Proteins", Vol. II, W. Lovenberg, Ed., Academic Press, New York, N.Y., 1973, Chapter 3; (b) W. Lovenberg in "Microbial Iron Metabolism", J. B. Neilands, Ed., Academic Press, New York, N.Y., 1974, Chapter 8.
(12) (a) J. A. Peterson and M. J. Coon, *J. Biol. Chem.*, **243**, 329 (1968); (b) E. T. Lode and M. J. Coon, *ibid.*, **246**, 791 (1971).
(13) W. D. Phillips, M. Poe, J. F. Weiher, C. C. McDonald, and W. Lovenberg, *Nature (London)*, **227**, 574 (1970).
(14) (a) W. Lovenberg and B. E. Sobel, *Proc. Natl. Acad. Sci. U.S.A.*, **54**, 193 (1965); (b) W. Lovenberg and W. M. Williams, *Biochemistry*, **8**, 141 (1969).
(15) (a) W. A. Eaton and W. Lovenberg, *J. Am. Chem. Soc.*, **92**, 7195 (1970); (b) W. A. Eaton, G. Palmer, J. A. Fee, T. Kimura, and W. Lovenberg, *Proc. Natl. Acad. Sci. U.S.A.*, **68**, 3015 (1971).
(16) D. D. Ulmer, B. Holmquist, and B. L. Vallee, *Biochem. Biophys. Res. Commun.*, **51**, 1054 (1973).
(17) (a) J. Peisach, W. E. Blumberg, E. T. Lode, and M. J. Coon, *J. Biol. Chem.*, **246**, 5877 (1971); (b) W. E. Blumberg and J. Peisach, *Ann. N.Y. Acad. Sci.*, **222**, 539 (1973).
(18) (a) K. K. Rao, M. C. W. Evans, R. Cammack, D. O. Hall, C. L. Thompson, P. J. Jackson, and C. E. Johnson, *Biochem. J.*, **129**, 1063 (1972); (b) C. L. Thompson, C. E. Johnson, D. P. E. Dickson, R. Cammack, D. O. Hall, U. Weser, and K. K. Rao, *ibid.*, **139**, 97 (1974).
(19) (a) K. D. Watenpaugh, L. C. Sieker, J. R. Herriott, and L. H. Jensen, *Acta Crystallogr., Sect. B*, **29**, 943 (1973); (b) L. H. Jensen in "Iron–Sulfur Proteins", Vol. II, W. Lovenberg, Ed., Academic Press, New York, N.Y., 1973, Chapter 4.
(20) (a) A. Davison and E. S. Switkes, *Inorg. Chem.*, **10**, 837 (1971); (b) A. Davison and D. L. Reger, *ibid.*, **10**, 1967 (1971).
(21) J. R. Anglin and A. Davison, *Inorg. Chem.*, **14**, 234 (1975).
(22) D. Coucouvanis, D. G. Holah, and F. J. Hollander, *Inorg. Chem.*, **14**, 2657 (1975).
(23) D. G. Holah and D. Coucouvanis, *J. Am. Chem. Soc.*, **97**, 6917 (1975).
(24) M. R. Churchill and J. Wormald, *Inorg. Chem.*, **10**, 1778 (1971).
(25) An x-ray diffraction study of $(Ph_4P)_2[Fe(SPh)_4]$ has established a distorted tetrahedral structure of the anion: D. Coucouvanis, D. Swenson, N. C. Baenziger, D. G. Holah, A. Kostikas, A. Simopoulos, and V. Petrouleas, *J. Am. Chem. Soc.*, **98**, 5721 (1976).
(26) R. W. Lane, J. A. Ibers, R. B. Frankel, and R. H. Holm, *Proc. Natl. Acad. Sci. U.S.A.*, **72**, 2868 (1975).
(27) N. S. Gill and F. B. Taylor, *Inorg. Synth.*, **9**, 136 (1967).
(28) S. J. La Placa and J. A. Ibers, *Acta Crystallogr.*, **18**, 511 (1965).
(29) See the paragraph regarding supplementary material at the end of this article.
(30) For a review, cf. C. A. McAuliffe and S. G. Murray, *Inorg. Chim. Acta Rev.*, **6**, 103 (1972).
(31) K. S. Murray and P. J. Newman, *Aust. J. Chem.*, **28**, 773 (1975).
(32) S. Jeannin, Y. Jeannin, and G. Lavigne, *J. Organomet. Chem.*, **40**, 187

(1972).
(33) (a) M. R. Snow and J. A. Ibers, *Inorg. Chem.*, **12**, 249 (1973); (b) T. Herskovitz, B. V. DePamphilis, W. O. Gillum, and R. H. Holm, *ibid.*, **14**, 1426 (1975).
(34) A similar lateral dimer structure has been established for the nonthiolate Fe(II) complex $[Fe(S_2CNEt_2)_2]_2$, whose nonbridging bite distance is ~2.9 Å compared to 3.16 Å in $[Fe_2(edt)_4]^{2-}$:[33a] O. A. Ileperuma and R. D. Feltham, *Inorg. Chem.*, **14**, 3042 (1975).
(35) Y. Sugiura, M. Kunishima, and H. Tanaka, *Biochem. Biophys. Res. Commun.*, **48**, 1400 (1972).
(36) (a) Y. Sugiura and H. Tanaka, *Biochem. Biophys. Res. Commun.*, **46**, 335 (1972); (b) Y. Sugiura, M. Kunishima, H. Tanaka, and H. H. Dearman, *J. Inorg. Nucl. Chem.*, **37**, 1511 (1975).
(37) (a) Because space group $Pn2_1a$ contains glide planes, the unit cell contains both enantiomers of each cation and anion, contrary to an earlier statement.[26] We thank Professor J. H. Enemark for pointing out this discrepancy. (b) A referee has raised the possibility that the crystal used for the structural determination may have contained some proportion of $[Fe(S_2\text{-}o\text{-}xyl)_2]^-$ with partial occupancy of site Y by a Na^+ counterion. In reply we note that Y is only 1.54 Å from X, an unreasonable distance for such a circumstance. Further, the root-mean-square amplitudes of vibration for the sulfur atoms in both structures (Table V) are comparable; an increase of these values in the $[Fe(S_2\text{-}o\text{-}xyl)_2]^{2-}$ structure would be expected if it were contaminated by $[Fe(S_2\text{-}o\text{-}xyl)_2]^-$.
(38) E. R. Brown and R. F. Large in "Techniques in Chemistry", Vol. I, Part IIA, A. Weissburger, Ed., Wiley-Interscience, New York, N.Y., 1971, Chapter VI.
(39) B. V. DePamphilis, B. A. Averill, T. Herskovitz, L. Que, Jr., and R. H. Holm, *J. Am. Chem. Soc.*, **96**, 4159 (1974).
(40) C. L. Hill, J. Renaud, R. H. Holm, and L. E. Mortenson, *J. Am. Chem. Soc.*, submitted for publication.
(41) W. M. Relff, I. E. Grey, A. Fan, Z. Ellezer, and H. Steinfink, *J. Solid State Chem.*, **13**, 32 (1975).
(42) A. Kostikas, V. Petrouleas, A. Simopoulos, D. Coucouvanis, and D. G. Holah, *Chem. Phys. Lett.*, **38**, 582 (1976).
(43) R. L. Collins, *J. Chem. Phys.*, **42**, 1072 (1965).
(44) J. R. Gabriel and S. L. Ruby, *Nucl. Instrum. Methods*, **36**, 23 (1965).
(45) W. Marshall and C. E. Johnson, *J. Phys. Radium*, **23**, 733 (1962).
(46) While quoting the approximate value $\Delta \sim 850$ cm^{-1} (used in Figure 7), Eaton and Lovenberg[11a] point out that their estimate of Δ ranges from 700 to 1100 cm^{-1}.
(47) J. V. Pivnichny and H. H. Brintzinger, *Inorg. Chem.*, **12**, 2839 (1973).
(48) L. Que, Jr., R. H. Holm, and L. E. Mortenson, *J. Am. Chem. Soc.*, **97**, 463 (1975); W. O. Gillum, L. E. Mortenson, J.-S. Chen, and R. H. Holm, *J. Am. Chem. Soc.*, in press.
(49) J. G. Norman, Jr., and S. C. Jackels, *J. Am. Chem. Soc.*, **97**, 3833 (1975).
(50) A brief discussion of Jørgensen's optical electronegativity concept as applied to the charge-transfer spectra of Rd_{red} and Rd_{ox} is given elsewhere: G. Palmer in "Iron–Sulfur Proteins", Vol. II, W. Lovenberg, Ed., Academic Press, New York, N.Y., 1973, Chapter 8.
(51) A. B. P. Lever, "Inorganic Electronic Spectroscopy", Elsevier, Amsterdam, 1968, Chapter 9.
(52) D. L. Leussing and J. Jayne, *J. Phys. Chem.*, **66**, 426 (1962).
(53) W. Hu and S. J. Lippard, *J. Am. Chem. Soc.*, **96**, 2366 (1974).
(54) F. A. Cotton, D. M. L. Goodgame, and M. Goodgame, *J. Am. Chem. Soc.*, **83**, 4690 (1961).
(55) However, the spectrochemical rankings of other, nonthiolate sulfur ligands may be more variable, but are still disposed toward the weak-field portion of the series: C. K. Jørgensen, *J. Inorg. Nucl. Chem.*, **24**, 1571 (1962); *Inorg. Chim. Acta Rev.*, **1**, 65 (1968).
(56) As was pointed out by a referee, side chain ligands *in combination* with other coordinating prosthetic groups may generate ligand fields sufficiently strong to pair spins (e.g., oxidized and reduced cytochrome *c*).
(57) G. A. Slack, F. S. Ham, and R. M. Chrenko, *Phys. Rev.*, **152**, 376 (1966).
(58) D. E. Drum and B. L. Vallee, *Biochem. Biophys. Res. Commun.*, **41**, 33 (1970); A. J. Sytkowski and B. L. Vallee, *Proc. Natl. Acad. Sci. U.S.A.*, **73**, 344 (1976).
(59) H. Eklund, B. Nordström, E. Zeppezauer, G. Söderlund, I. Ohlsson, T. Boiwe, and C.-I. Brändén, *FEBS Lett.*, **44**, 200 (1974).
(60) D. R. McMillan, R. A. Holwerda, and H. B. Gray, *Proc. Natl. Acad. Sci. U.S.A.*, **71**, 1339 (1974).
(61) Cf., e.g., E. I. Solomon, P. J. Clendening, H. B. Gray, and F. J. Grunthaner, *J. Am. Chem. Soc.*, **97**, 3878 (1975); E. I. Solomon, J. W. Hare, and H. B. Gray, *Proc. Natl. Acad. Sci. U.S.A.*, **73**, 1389 (1976).
(62) Attempts to prepare Cu(II)–S_2-*o*-xyl complexes have thus far yielded as stable products white solids containing Cu(I).
(63) This complex would presumably be analogous to diamagnetic, structurally characterized $[Ni_3(SCH_2CH_2NH_2)_4]^{2+}$: C.-H. Wei and L. F. Dahl, *Inorg. Chem.*, **9**, 1878 (1970).
(64) G. A. Barclay, E. M. McPartlin, and N. C. Stephenson, *Acta Crystallogr., Sect. B*, **25**, 1262 (1969); A. C. Villa, A. G. Manfredotti, M. Nardelli, and C. Pelizzi, *Chem. Commun.*, 1322 (1970).
(65) R. H. Holm and M. J. O'Connor, *Prog. Inorg. Chem.*, **14**, 241 (1971).
(66) M. R. Churchill, J. Cooke, J. P. Fennessey, and J. Wormald, *Inorg. Chem.*, **10**, 1031 (1971).
(67) B. L. Vallee and R. J. P. Williams, *Proc. Natl. Acad. Sci. U.S.A.*, **59**, 498 (1968).
(68) R. G. Shulman, P. Eisenberger, W. E. Blumberg, and N. A. Stombaugh, *Proc. Natl. Acad. Sci. U.S.A.*, **72**, 4003 (1975).
(69) D. E. Sayers, E. A. Stern, and J. R. Herriott, *J. Chem. Phys.*, **64**, 427 (1976).
(70) L. E. Bennett, *Prog. Inorg. Chem.*, **18**, 1 (1973).
(71) N. Sutin in "Inorganic Biochemistry", Vol. 2, G. L. Eichhorn, Ed., Elsevier, Amsterdam, 1973, Chapter 19.
(72) R. J. P. Williams, *Inorg. Chim. Acta Rev.*, **5**, 137 (1971).
(73) J. W. Lauher and J. A. Ibers, *Inorg. Chem.*, **14**, 348 (1975); T. J. Kistenmacher and G. D. Stucky, *ibid.*, **7**, 2150 (1968); F. A. Cotton and C. A. Murillo, *ibid.*, **14**, 2467 (1975).
(74) A value of 0.05 Å for *P. aerogenes* Rd_{red}/Rd_{ox} has been estimated from EXAFS analysis.[68]
(75) C. A. Jacks, L. E. Bennett, W. N. Raymond, and W. Lovenberg, *Proc. Natl. Acad. Sci. U.S.A.*, **71**, 1118 (1974).
(76) Cf., e.g., H. C. Stynes and J. A. Ibers, *Inorg. Chem.*, **10**, 2304 (1971), and references cited therein; H. Taube, "electron Transfer Reactions of Complex Ions in Solution", Academic Press, New York, N.Y., 1970, Chapter II.

Phase-Transfer Catalyzed and Two-Phase Reactions of Aromatic Nitro Compounds with Iron Carbonyls

Hervé des Abbayes and Howard Alper*

Contribution from the Department of Chemistry, University of Ottawa, Ottawa, Ontario, Canada K1N 6N5. *Received June 14, 1976*

Abstract: The first examples of the application of phase-transfer catalysis to metal carbonyl chemistry are described. Anilines were formed in good to excellent yields by treatment of nitro arenes with triiron dodecacarbonyl, aqueous sodium hydroxide, benzene, and benzyltriethylammonium chloride as the catalyst (room temperature, 0.75–2.0 h). A mechanism is proposed involving $HFe_3(CO)_{11}^-$ as a key intermediate. The reduction of nitro compounds can also be effected using $Fe(CO)_5$ (or $Fe_2(CO)_9$) in place of $Fe_3(CO)_{12}$, but the catalyst is not required. Steric and electronic effects are significantly different in the $Fe_3(CO)_{12}$ and $Fe(CO)_5$ reactions.

There have been many important applications of phase-transfer catalysis in synthetic organic chemistry during the past few years (e.g., carbene reactions).[1] It seemed conceivable to us that the process should also be useful in transition metal organometallic chemistry, particularly for reactions involving anionic species. This paper describes the first application of phase-transfer catalysis to metal carbonyl chemistry.[2]

Iron carbonyl hydrides $[HFe(CO)_4^-$, $HFe_3(CO)_{11}^-]$ are useful reagents for effecting reductive amination,[3-5] alkylation,[6,7] hydroacylation,[8] dehalogenation,[9] and for reduction of nitroarenes,[10,11] Schiff bases,[12] diazines,[12] and α,β-unsaturated carbonyls.[13] As these hydrides can be generated by reaction of the appropriate iron carbonyl with hydroxide ion or methanol, they appeared to be excellent models for testing